Text Note S1

A. Geochronology and stratigraphy

KSD-VP-1/1 was recovered from mudstone at the base of an exposure of upward coarsening claystone, siltstone and sandstone nearly 1 m thick (see Figure S2). Laterally, this upward coarsening succession is incised and overlain by channel-fill conglomerate and sandstone (Figure S2). A trench excavated about 25 m from the fossil locality reveals more than 2.5 m of claystone, siltstone and sandstone below the fossil horizon (see Figure S3). A tuff at the base of the trench has been dated by the $^{40}Ar/^{39}Ar$ method, yielding an age of 3.60 ± 0.03 Ma (2σ; see Figure S4 and Table S2)[1]. All strata in this section comprise a single normal magnetozone (see below for details). Samples with previously reported reverse magnetization[2] are from an adjacent fault block with older stratigraphic units (see Figure S2). The simplest interpretation of the age and reversal data is that the bottom of the trench lies at or just above the Gauss/Gilbert paleomagnetic transition, with the normal magnetozone equating with the lower part of the normal subchron C2An.3n (3.596–3.330 Ma[3]). Using nominal sedimentation rates (11 cm/ky overall for strata ~3.8–3.6 Ma in this area[1]), the fossil specimen KSD-VP-1/1, found 2.6 m above the dated tuff, has an estimated age of 3.58 Ma.

B. Paleomagnetic samples and results

Nine oriented blocks for paleomagnetic analysis (KSD09-1 to KSD09-9) were collected from claystone and siltstone strata in a 3m deep trench 25 m from KSD-VP-1/1 partial skeleton at 11º28'54.5''N, 40º30'39.8''E. Three specimens were cut from each block and the natural remanent magnetization (NRM) measured at the Berkeley Geochronology Center, using alternating field (AF) followed by thermal demagnetization at ~50ºC steps to 605ºC (for further discussion of technique see 1). All samples exhibit normal remanence directions, though some (KSD09-1, 09-3 and 09-7) show a reverse overprint typically removed during AF and thermal demagnetization (Figures S4-S5). In a few specimens, the secondary reverse magnetization was not completely removed during the demagnetization procedure, leading to ambiguous polarity determinations. In these cases, new specimens were cut from the original sample blocks, selecting the finest grained material. For KSD09-1, the new specimens yielded unambiguous normal polarity. KSD09-7 showed normal declinations but shallow negative inclinations interpreted as a later, secondary overprint. Some specimens of KSD09-3 showed initial reverse directions that shifted to normal during the demagnetization process, with just a single specimen retaining reversed polarity after demagnetization. We conclude that all sedimentary rocks in the trench were deposited during a period of normal polarity (Figure S5).

Text Note S2

The anterior inferior iliac spine (AIIS) is massive and defines the upper border of a deep iliopsoas groove (Figure S6). The ilium is thickened posterior to it, and while much of its crest is missing, the preserved portion (i.e., the "iliac pillar") is located more anteriorly than its human homologue, consistent with lateral iliac flare typical of *Australopithecus*[4] .

The greater sciatic notch is well-demarcated and narrow, and is much more acute than that of A.L. 288-1 or Sts 14. The notch is substantially obtuse in two obvious female *Australopithecus*, but narrowed and more acute in KSD-VP-1/1. A platypelloid pelvis would not prevent selection for anteroposterior expansion of the birth canal. Was selection for AP birth canal already present in *Australopithecus*? The shape of the sciatic notch in the recently described BSN49/P27 pelvis, assigned to *H. erectus*, is relevant in this regard (see Figure S9). The ischial spine of KSD-VP-1/1 has been sheared away and a comparable value must therefore be estimated, but must have been between 0.20 and 0.25, below the human female range (*ca* 0.28-0.53) and well within the modern male range (*ca* 0.08-0.43). A.L. 288-1 and Sts 14 are 0.29 and 0.38, respectively. The former value lies within the range of overlap of human males and females, while Sts 14's value is well above the modern male range.
The acetabulum has a well-formed lunate surface with a more substantial anterior extension than in A.L. 288-1. A portion of the superior pubic ramus is preserved, but has been compressed inferiorly, artificially reducing the acetabulum's diameter. Consistent with hip mechanics in *Australopithecus*[4], an estimate of the original acetabulum appears somewhat small (vertical acetabular diameter ≈ 49 mm); i.e., it is about 14% of tibial length (see also below).

Text Note S3

Ape distal tibial metaphyses are demonstrably broad and rectangular, primarily reflecting their more massive medial malleoli and expanded anterior plafonds[5,6]. Overall metaphyseal dimensions are unaffected by the specimen's pathology. Its AP/ML ratio (100) is decidedly hominid as is its probable malleolar index (= 47)(Table S7). Simple visual inspection shows the plafond to be remarkably narrow and largely square, rather than rectangular as in African apes (Figure S12). All of these features confirm a lack of any significant adaptation to vertical climbing[5,6], as is the case with all early hominids.

KSD-VP-1/1e exhibits only one non-hominid character, a lateral declination of the distal articular surface (Table S7). Whereas the plafond/shaft angle is 90° in humans[5], it is 100° in KSD-VP-1/1e. However, thirteen other early hominids have human-like values[5], and fibular fracture (see earlier) is known to lead to lateral declination of the plafond[7] as in KSD-VP-1/1e.

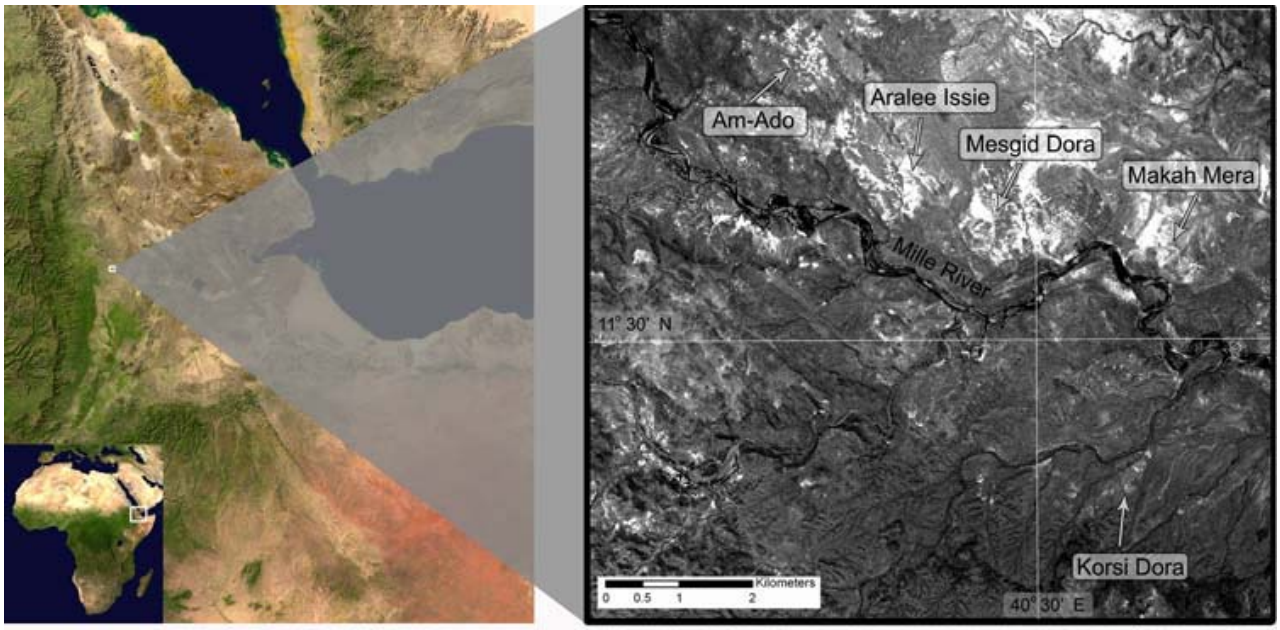

Figure S1. Satellite imagery location map of the Woranso-Mille study area. Korsi Dora is the locality where the partial skeleton (KSD-VP-1/1) was found. Other fossil collection areas are indicated.

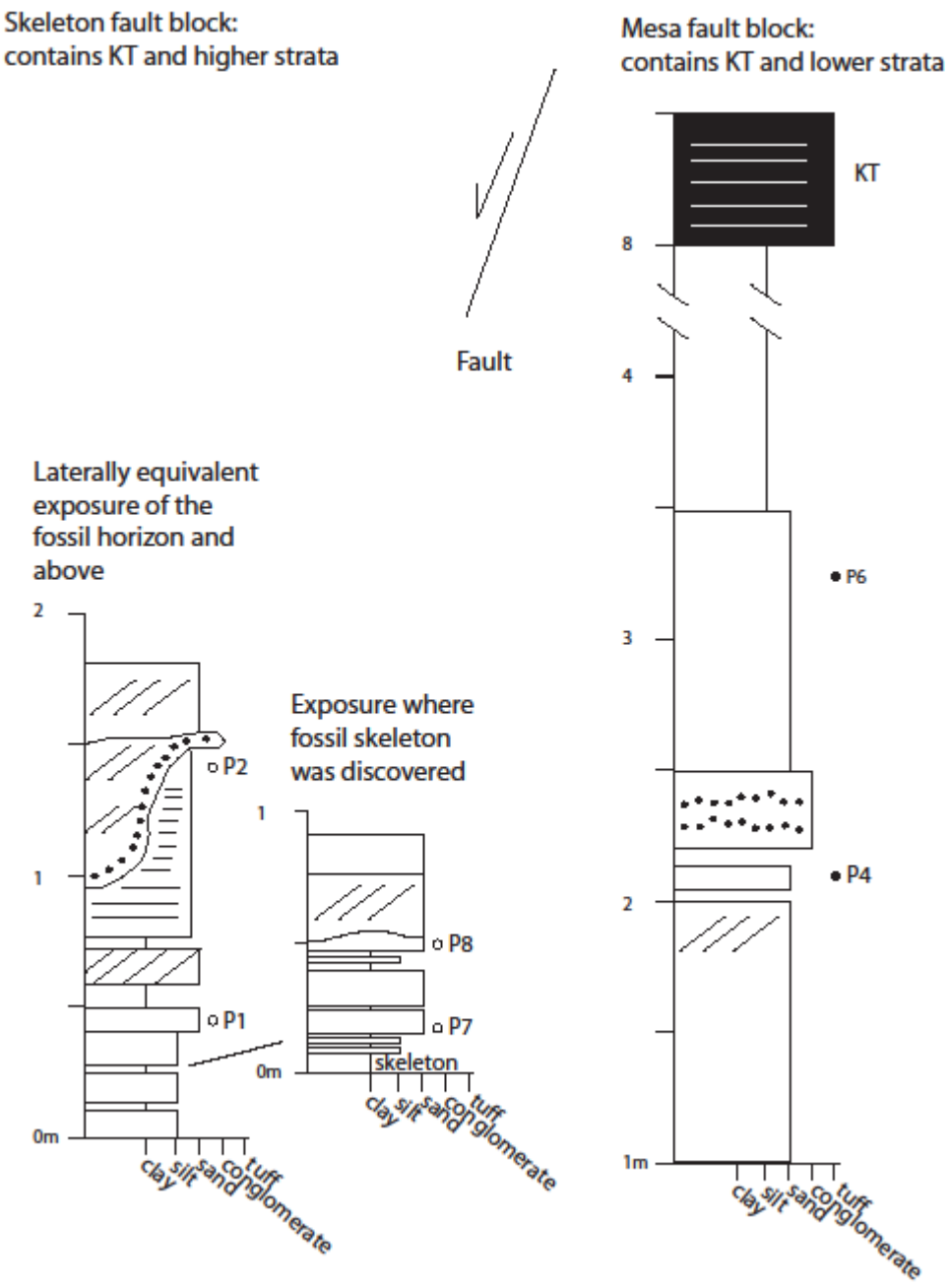

Figure S2. Stratigraphic columns showing the positions of samples for which paleomagnetic data were previously published[1]. Solid circles indicate samples with reverse magnetization, all of which lie below the Kilaytoli Tuff (KT). Open circles indicate samples with normal magnetization, all from a different fault block than the reverse magnetized samples, and stratigraphically above the KT. Samples from both fault blocks were previously plotted, mistakenly, on a single composite section[1].

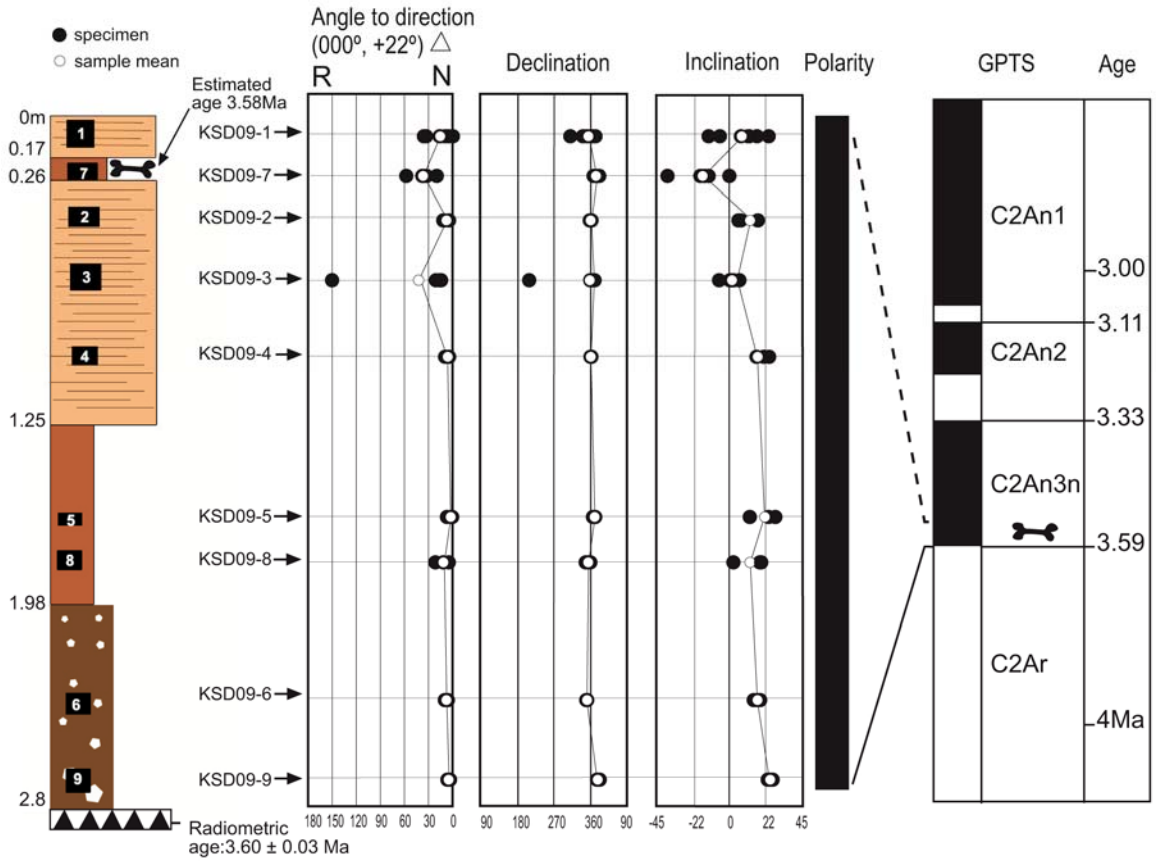

Figure S3. Paleomagnetic results for nine samples collected along the excavated trench 25 m from the fossil site. Paleomagnetic directions show the angular distance (delta) to the expected normal direction (000º, 22) for this latitude. The stratigraphic position of the fossil skeleton horizon is indicated by the bone symbol. All samples exhibit normal remanence directions, with mean declinations towards the magnetic north, though some specimens in samples (KSD09-1, 09-3 and 09-7) show a reverse overprint producing shallow negative inclinations with a small delta value. A tuff at the base of this sequence has been dated by the $^{40}Ar/^{39}Ar$ method, yielding an age of 3.60 ± 0.03 Ma and all strata in this 3m section comprise a single normal magnetozone. The simplest interpretation is that the bottom of the trench lies at or just above the Gauss/Gilbert paleomagnetic transition, with the normal magnetozone equating with the lower part of the normal subchron C2An.3n (3.596–3.330 Mtea[2]). Using nominal sedimentation rates (11 cm/ky overall for strata ~3.8–3.6 Ma in this area[1]), the fossil specimen KSD-VP-1/1, found 2.8 m above the dated tuff, has an estimated age of 3.58 Ma.

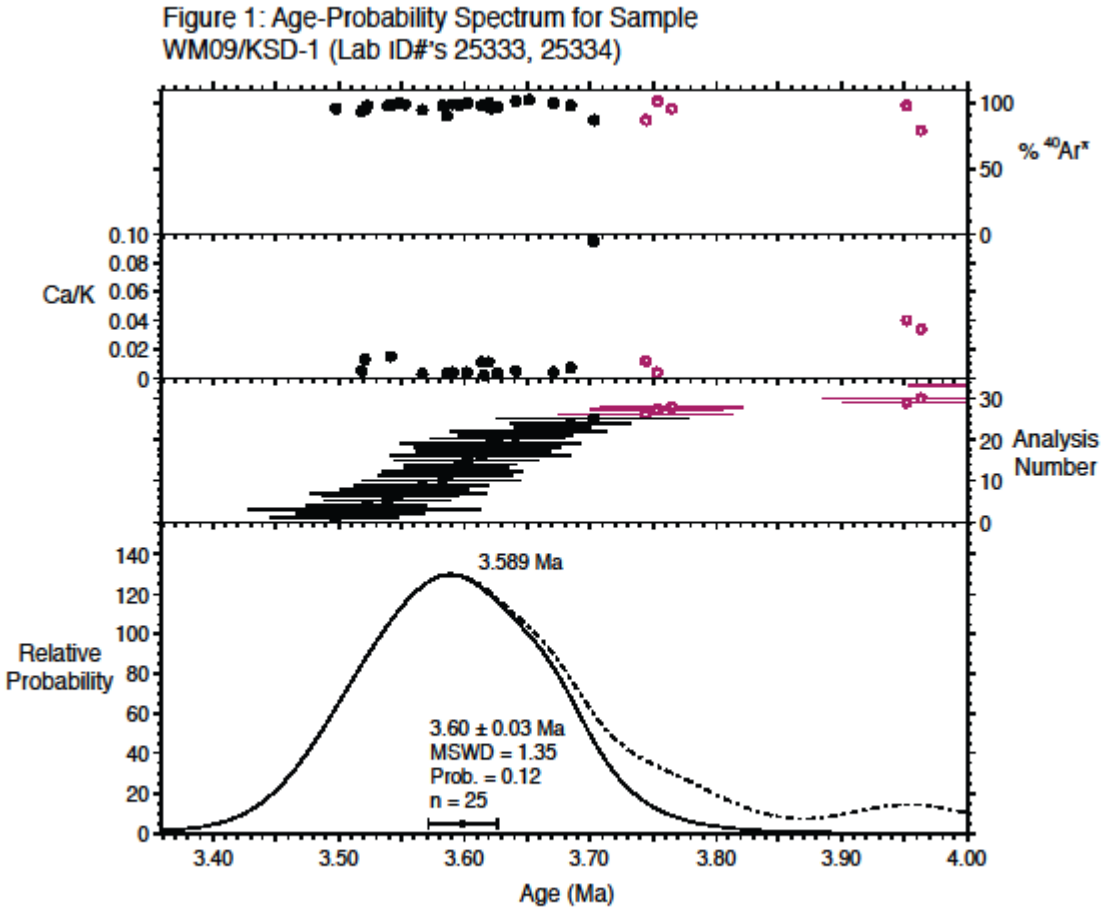

Figure S4. Age-Probability Spectrum for Sample WM09/KSD-1 (Lab ID#s 25333, 25334).

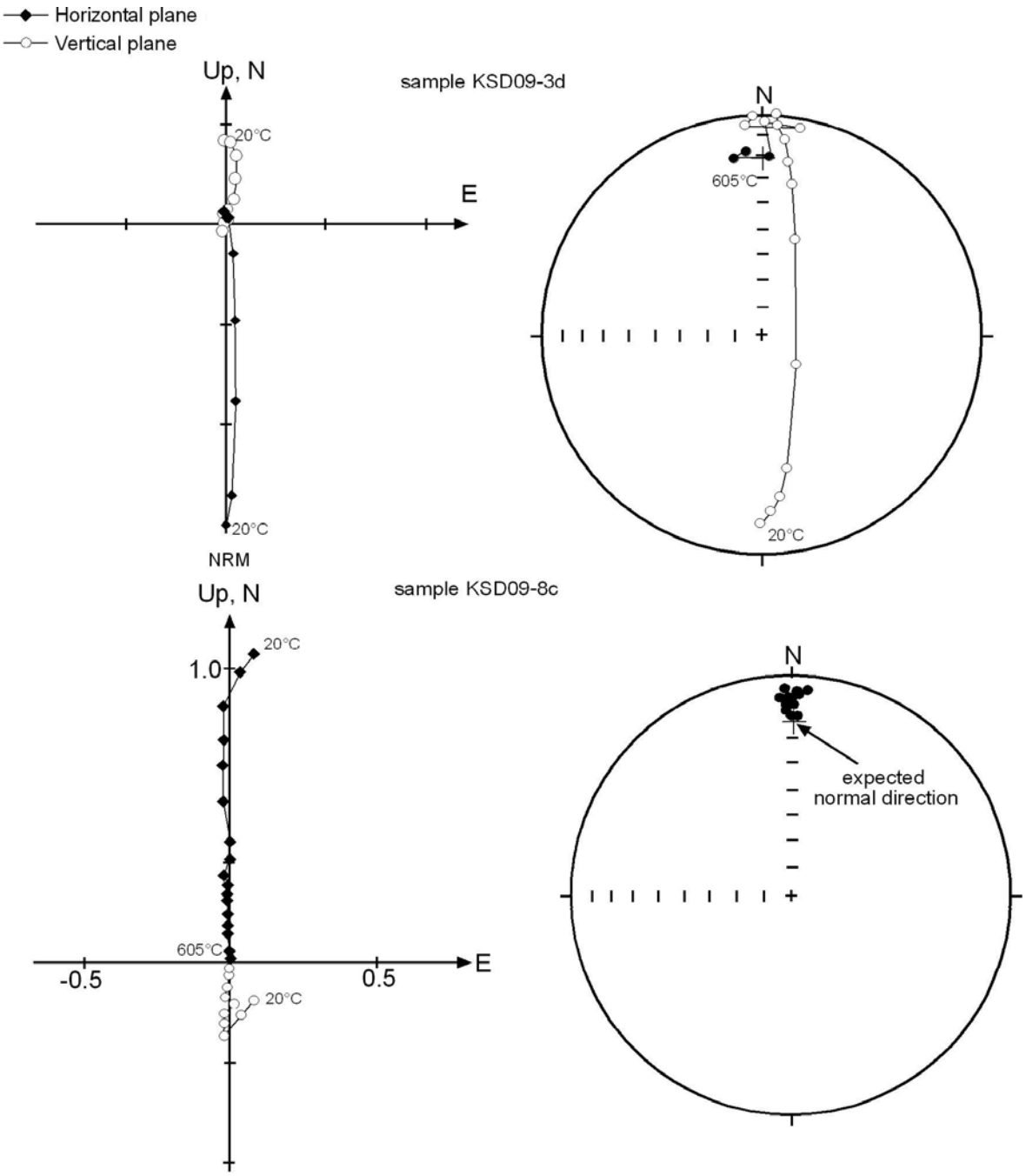

Figure S5. Orthogonal and stereographic plots showing directions at different steps of demagnetization for specimens KSD09-3d and KSD09-8c. Removal of a reverse directed magnetization occurs in specimen KSD09-3d showing initial reverse directions that change to normal during demagnetization. Specimen KSD09-8c shows only normal directions.

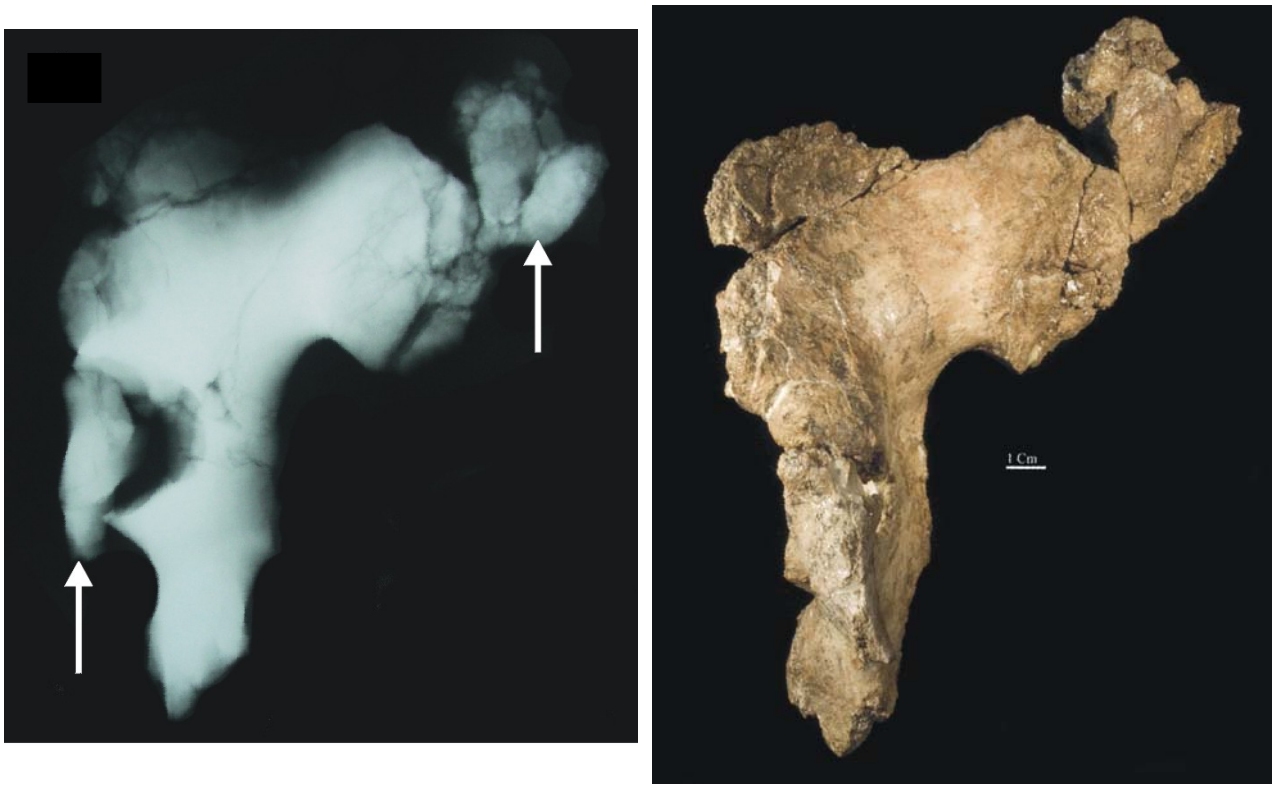

Figure S6. Anteroposterior X-ray of KSD-VP-1/1d (left) and AP View of the Specimen (right). The radiograph was taken prior to partial repositioning of some fragments in the laboratory following removal of matrix, and the orientation of these two illustrations varies slightly. Note the broken and translated superior pubic ramus (white arrow on left) and the somewhat ovoid appearance of the acetabulum. Its elongated mediolateral transect is a consequence of superoinferior compression--the same damage that has caused the fragmentation of the superior pubic ramus. Note also the translation of a substantial portion of the retroauricular region (white arrow on the right). Although this fragment has been relocated since the X-ray, it nevertheless still lies considerably superior to its original location, and has resulted in superior repositioning of a major portion of the retroauricular region (including the PSIS) even after this repair. This has elevated the posterior iliac crest to some extent. For discussion see text.

Figure S7. Superior (left) and Anterior Views (right) of KSD-VP-1/1t. The alae are unusually broad as in other sacra of *Australopithecus* (cf., Figure S10).

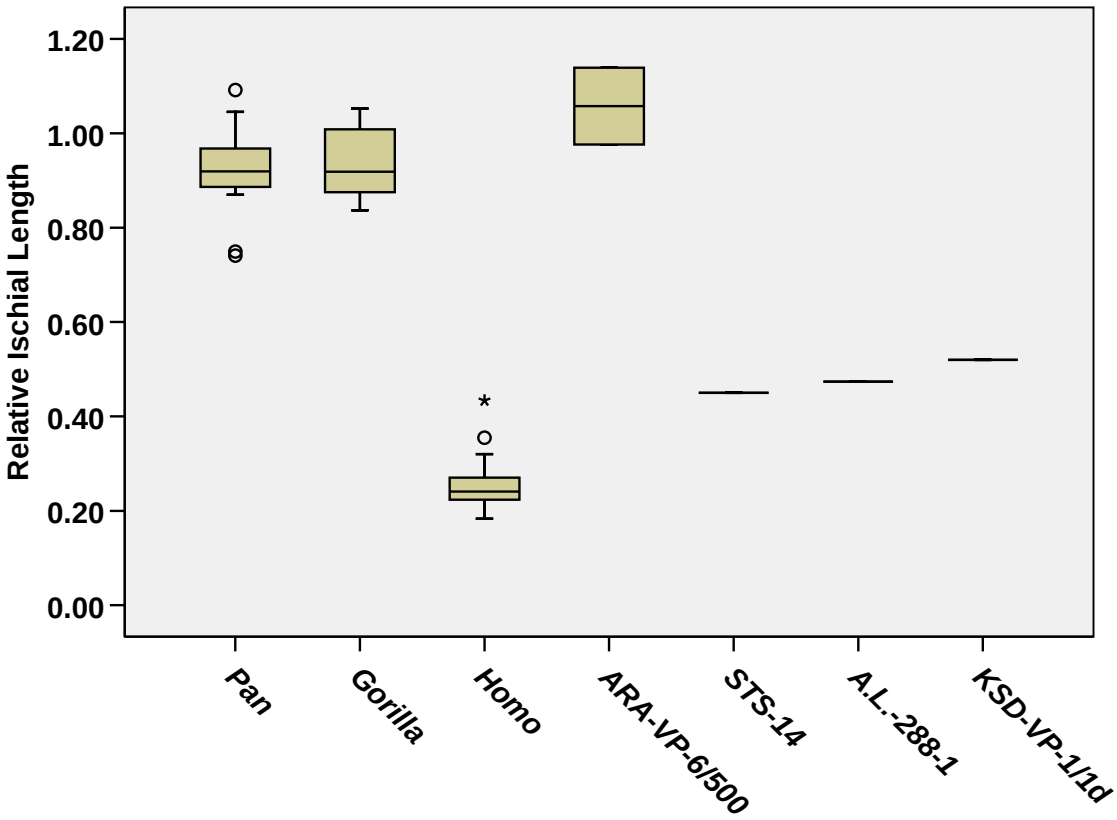

Figure S8. Relative Ischial Length in KSD-VP-1/1d and Extant Hominoids. The minimum distance between the lower rim of the acetabulum and the superomost point on the ischial tuberosity has been divided by the acetabular diameter for samples of extant hominoids (N = 25 each species). The positions of the three *Australopithecus* specimens are close to those of *Homo*, but still lie slightly outside the range of the sample shown here, although this ratio in other human samples sometimes overlaps those of *Australopithecus*. At least some of this difference is a consequence of expansion of the diameter of the acetabulum in *Homo*. Values for *Ar. ramidus* (ARA-VP-6/500) are from the original specimen, but normalized by estimates of the probable maximum and minimum of acetabulum diameter. Each box shows the median, interquartile range (the box length), outliers (open circles) and extreme values (asterisks) within a category. Outliers are cases with values between 1.5 and 3 box lengths from the upper or lower edge of the box. Extreme values are those with values more than 3 box lengths from the upper or lower edge of the box.

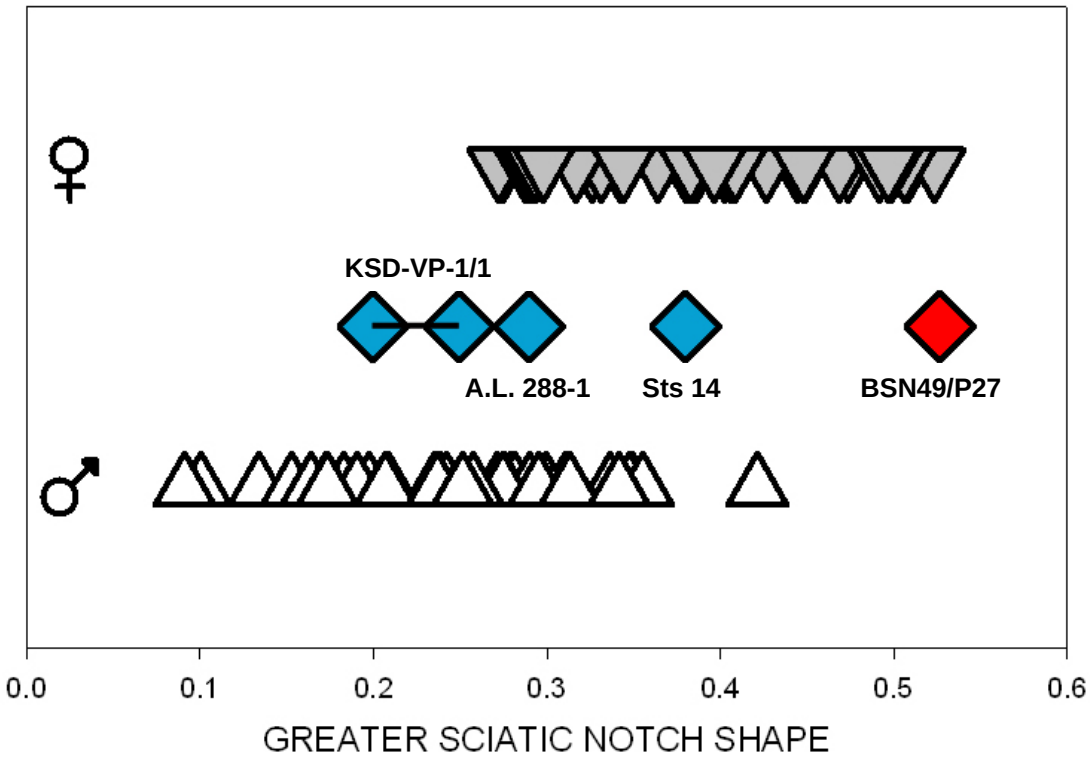

Figure S9. Plot of Estimated Angulation of Sciatic Notch. The shape of the greater sciatic notch is shown here graphically using the method and data of Simpson *et al.*[8]. That sample is composed of 20 females and 20 males from the Hamann-Todd collection, Cleveland Museum of Natural History. The horizontal axis is the range of values of the position of the deepest part of the notch relative to the "sacro-iliac tubercle along a line connecting the ischial spine to the tubercle for the inferior sacro-iliac ligament. A value of 0.5 indicates that the inflection point is located midway along a line defining the opening of the [greater sciatic notch]". A range of possible values is shown for KSD-VP-1/1 (connected by horizontal line). Values for A.L. 288-1, Sts-14, and BSN49/P27 are also shown. Body size suggests that KSD-VP-1/1 is male, while it is reasonably certain that A.L. 288-1 is female based on the same criterion (see also 9). These data may require reassessment of the assumption that pelvic dimorphism is not detectable in early hominids on the basis of pelvic morphological characters. Figure courtesy of S. Simpson.

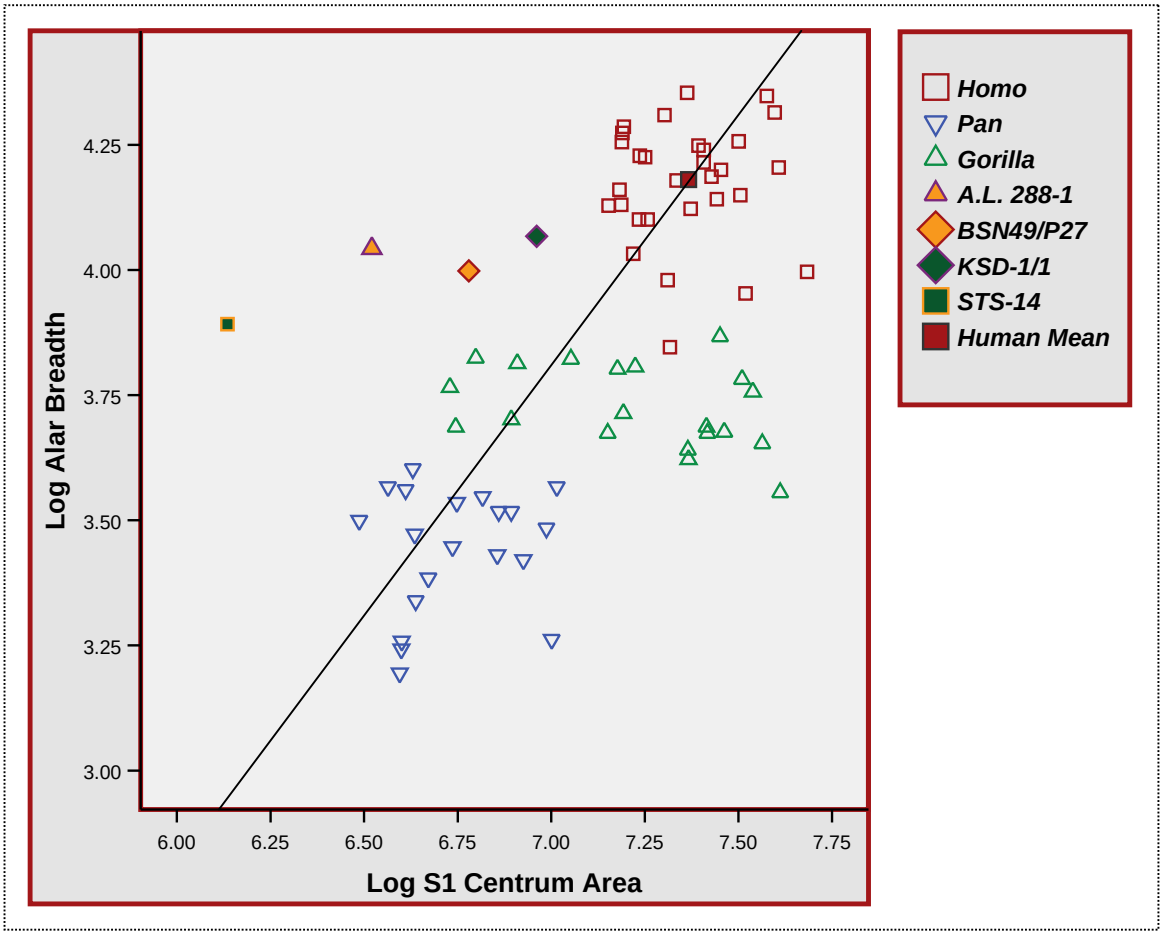

Figure S10. Natural Log-Log Scatterplot of Relative Alar Breadth (both alae) of the Sacrum in *Australopithecus* and Extant Hominoids. Alar breadth was calculated as the maximum breadth of the sacrum less the transverse diameter of the S1 centrum. S1 centrum area was calculated as the product of its AP and ML dimensions. The human mean has also been plotted. Other symbols are provided in the legend. KSD-VP-1/1 lies nearer the human cloud than do A.L. 288-1 and Sts-14, which may be an allometric effect of these smaller examples of *Australopithecus*. Data for Sts-14 from Robinson[10]. Data for BSN49/P27 from the Simpson, *et al.* reconstruction[8].

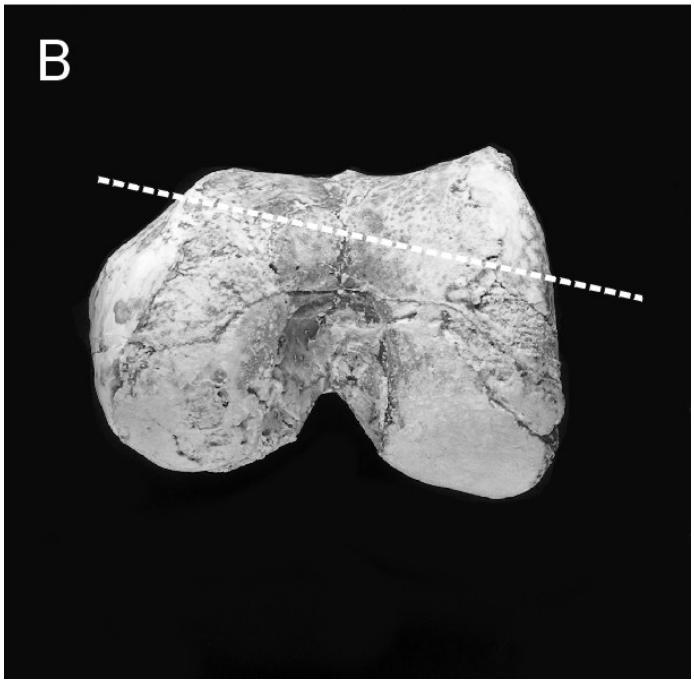

Figure S11. Lateral (A) and Distal (B) Views of KSD-VP-1/1c. Both views are reproduced here in Black & White to highlight surface contrast. In **A,** material has been added between various cracks in order to stabilize the specimen, but the specimen's original dimensions were preserved by underlying cancellous bone. The condylar outline is decidedly elliptical, although the shape index[11] falls approximately between human and chimpanzee distributions (see also text).

B. The medial condyle is somewhat foreshortened by postmortem damage but its relationship to the lateral condyle is reasonably well preserved. A dashed line has been inscribed connecting the locations of the medial and lateral meniscal grooves. The lateral condyle's meniscal groove is difficult to locate because of surface damage, but the inscribed line passes through a distinct depression, which although eroded, was its probable location. Tibial position in full extension, as defined by this line (see also 11), shows a very high lateral lip to the patellar groove, suggesting a long period of substantial selection for a knee joint habitually placed in valgus during stance phase.

Figure S12. A. Lateral (A) and Inferior (B) Views of Distal End of KSD-VP-1/1e. Photographs A and B are reproduced here in Black & White to highlight surface contrast. **A**. A continuous perimeter of reactive bone surrounds the fibular facet. Its superior course has been marked by black arrows. The bony outgrowth has elongated tibial length by about one cm. This is most likely due to a remote, non-united fibular fracture.

B. Inferior view shows a distal projection of the bony outgrowth (bracket) and the severed medial malleolus (arrow). The form of the malleolus, however, can be deduced because of its near-surgical transection. Despite the effects of the fracture, the markedly concave tibial plafond is still evident in **A**, though metric assessment requires caution because of the efflorescence of reactive bone. For further discussion see text.

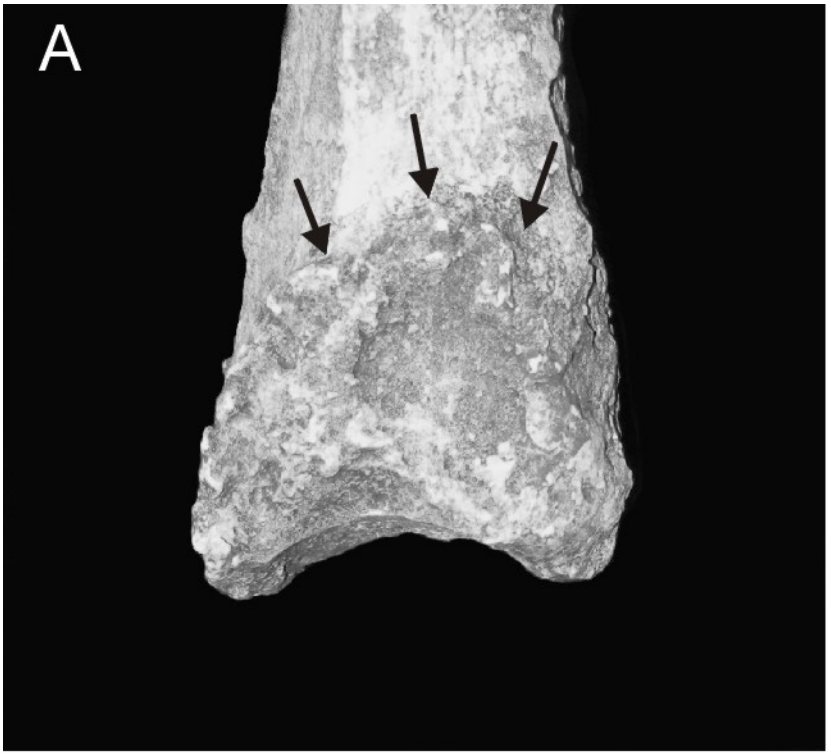

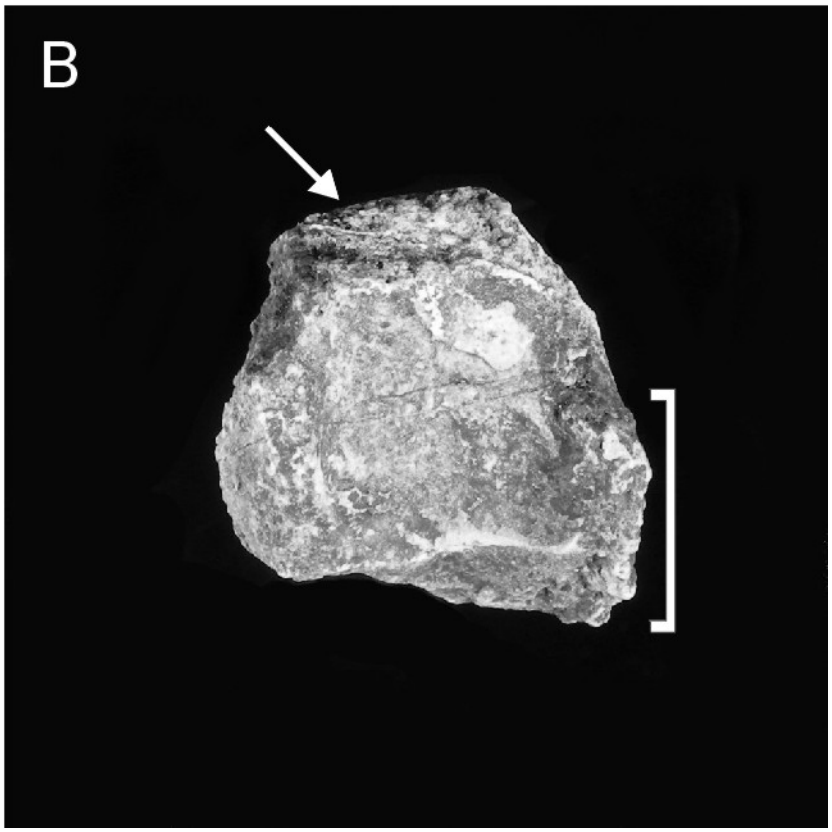

Figure S13. KSD-VP-1/1e is nearly complete for its entire length (from well above the apex of the tibial tuberosity [arrow] proximally to the plafond surface distally), making length estimation very accurate, as only the intercondylar eminence is missing from some standard length measures, i.e., physiological length. The shaft has spalled and been compressed mediolaterally, but was nevertheless clearly platycnemic. Maximum Length = 355; Physiological Length = 343.For discussion see text.

Figure S14. Ribs Recovered from KSD-VP-1/1. Close-ups and drawings of the second rib are provided in Figures S15-S17. Specimens shown here (top to bottom) are KSD-VP-1/1n (left second rib; reversed), KSD-VP-1/1q (right 5th, 6th, or 7th rib), KSD-VP-1/1s (middle rib fragment), KSD-VP-1/1o (right 7th or 8th rib), KSD-VP-1/1p (right 8th or 9th rib), and KSD-VP-1/1r (left 11th rib). See also, Table S1.

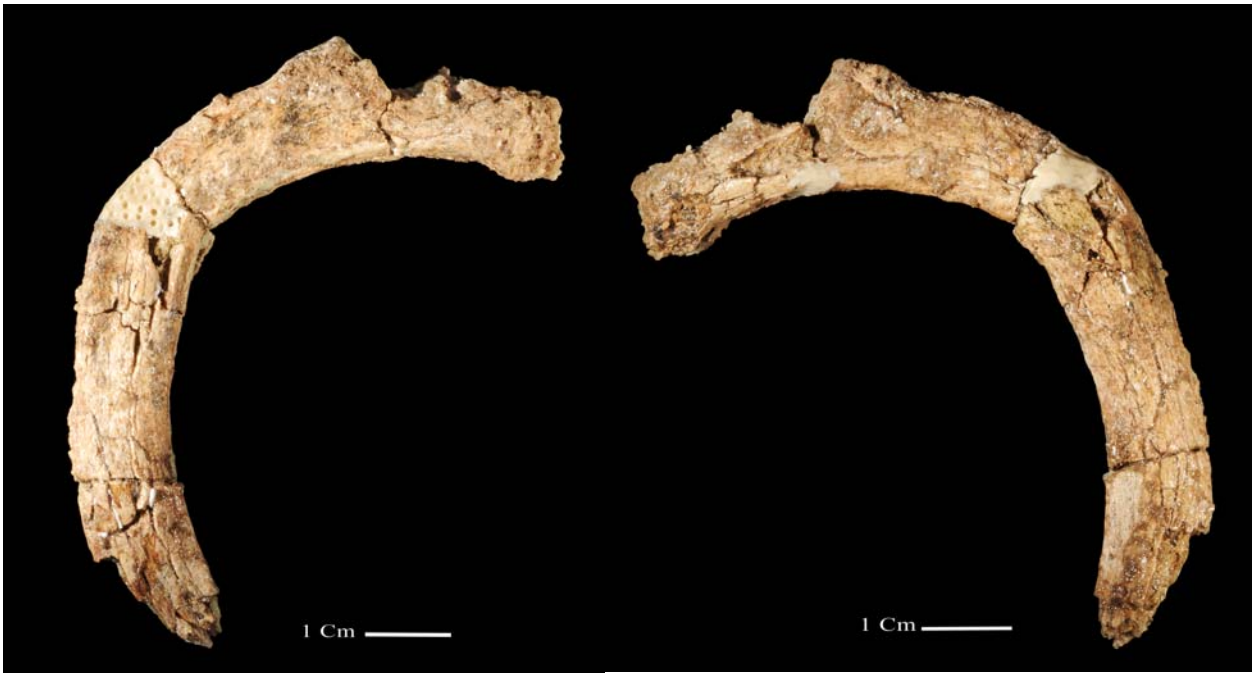

Figure S15. Inferior (left) and Superior (right) Views of Left Second Rib. The rib's geometry is well preserved and its head also preserves its fundamental morphology. Slight postmortem damage at the point of reinforcement shown in both views may have slightly increased the rib's curvature (and thereby decreased estimates of original cupola volume). The specimen, however, is sufficiently complete to allow reliable assessment of curvature as shown in Figure S16-S17. Results of this assessment (Figure 2) place its curvature well within the human range and substantially below values of this index for most African apes. For additional discussion see the legends of Figure S16-S17 and the text.

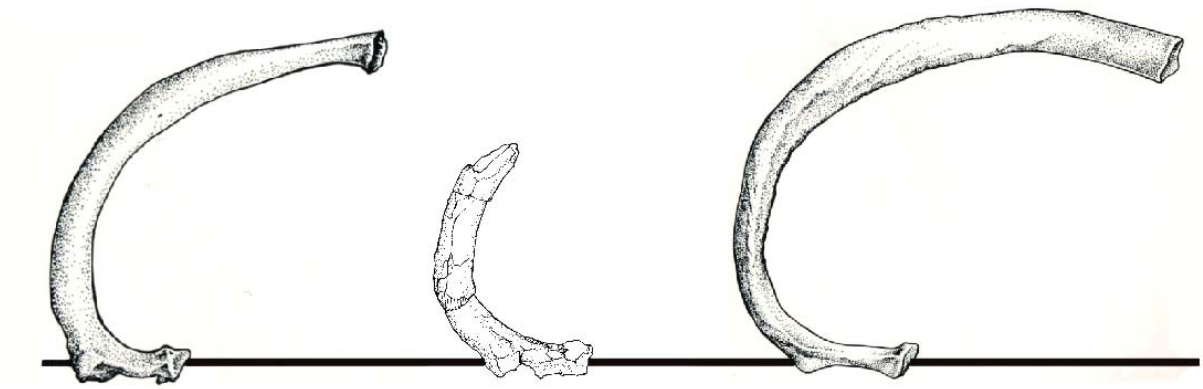

Figure S16. Second Ribs of Hominoids Aligned on their Costal Neck Axis and Size Normalized. The second ribs of a chimpanzee (left), KSD-VP-1/1 (center), and a modern human (right) have been aligned on their costal neck axis[12], and scaled to the same interfacet distance (distance A in Figure S17). Although the specimen from KSD-VP-1/1 is incomplete, enough of its original length was recovered to preserve the likely trajectory of its overall curvature, which is not constricted like that of *Pan*, and is therefore more similar to that of *Homo*. This can be quantitatively assessed using the index described in Figure S17. Results of that method are presented in Figure 2. The human and chimpanzee specimens have been redrawn from 12.

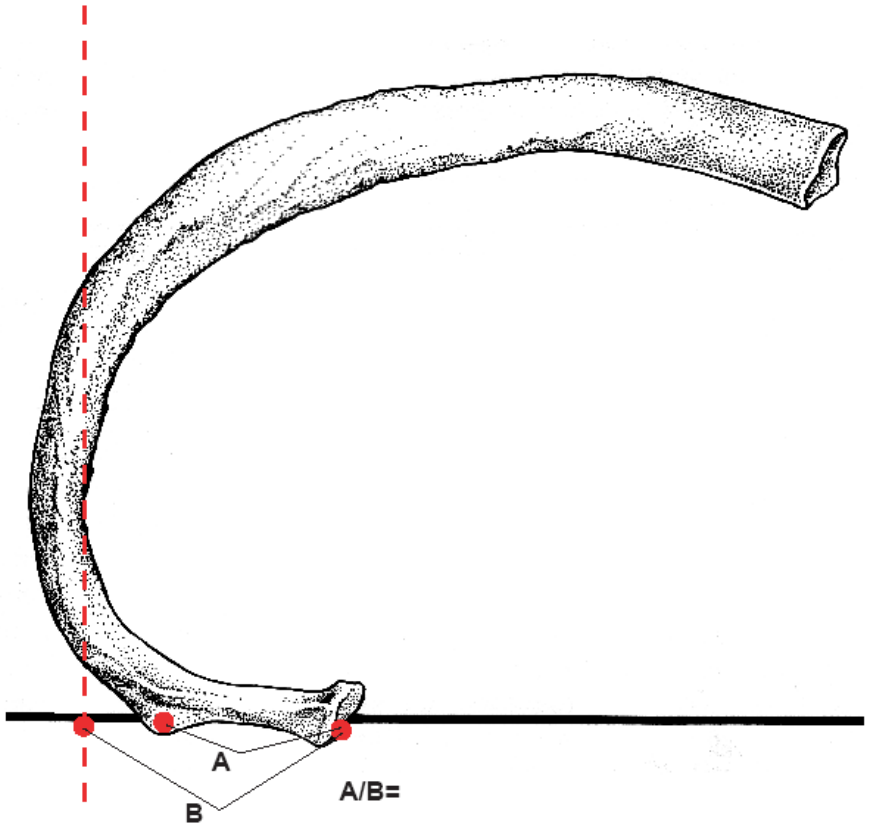

Figure S17. Method Used for Assessing Second Rib Curvature Index in Hominoids (cf., Figures 2 and S14-S16). A line is first drawn connecting the centroids of the two articular facets of the rib (for the centrum and for the transverse process of its associated vertebra); the "costal neck axis" (see 12 for more details). A line is then inscribed perpendicular to that line and which also lies tangent to the most lateral point on the pleural surface of the rib. Two distances are measured: one between the centroids of the two facets (A) and one between the centrum's facet and the intersection of the inscribed perpendicular with the costal neck axis (B). The Rib Curvature Index is then calculated as A/B X 100. Data for hominoids are shown in Figure 2 (*Homo* N = 13; *Gorilla* N = 33; *Pan* N = 16). The African ape and human ranges overlap only minimally; i.e., only one *Gorilla* value (65) fell within the human range, all others exceeded it. The value for KSD-VP-1/1n was 66.

Figure S18. Superior (above) and Inferior (below) Views of the Left Clavicle (KSD-VP-1/1f). Both sternal and acromial ends have suffered bone loss (for discussion see text). Comparisons of regressed clavicle length to various individual upper and lower limb dimensions (Figure S19) show that KSD-VP-1/1f falls consistently with *Homo* and not with either African ape. In conjunction with the specimen's second rib, these data confirm that early hominids lacked the constricted cupola of African apes.

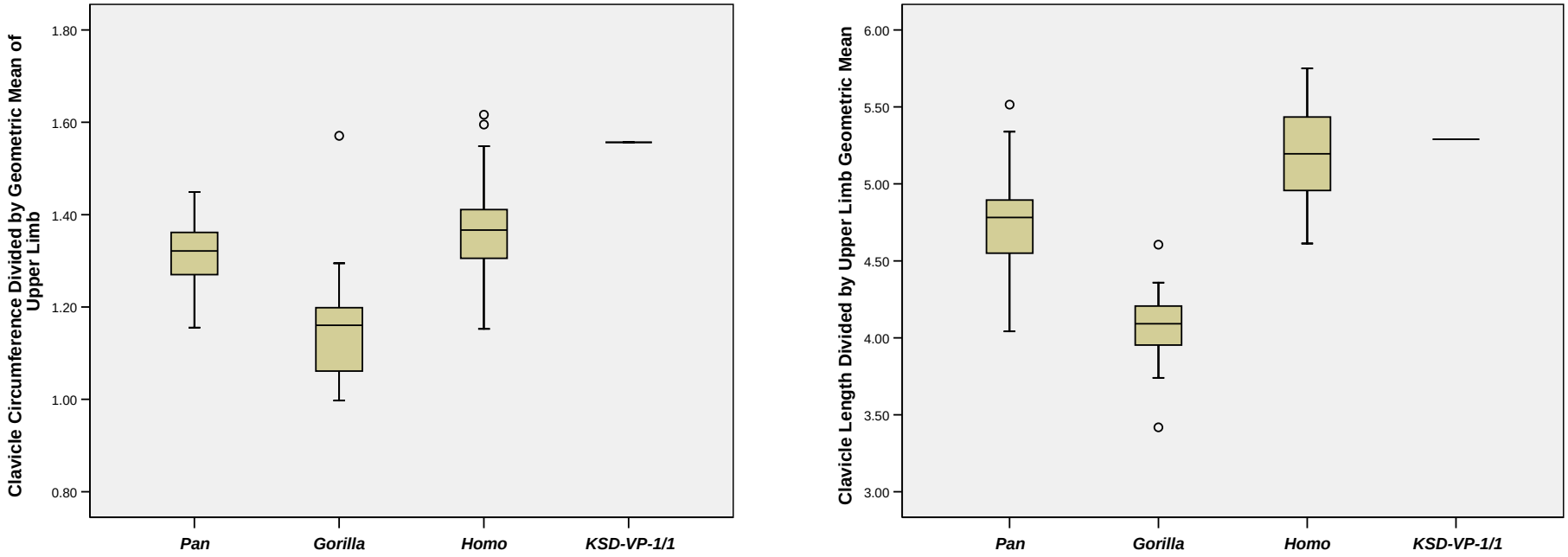

Figure S19. Box plots of Relative Clavicle Circumference and Length. Clavicular circumference (**left**) and length (**right**) have been divided by the geometric mean of eight upper limb joint dimensions (see Figures S28-S30). Note that relative clavicular circumference in KSD-VP-1/1 exceeds the range in African apes and falls near the upper limit of *Homo*. The latter is not surprising as the human antebrachium has undergone significant reduction relative to its length since BOU-VP-12/1[13]. Regressed clavicle length lies closer to the human median; however, comparison of this length estimate (156 mm) to the actual specimen suggests that it may be an underestimate. Exfoliation at the midshaft of KSD-VP-1/1f also makes the regressed length an underestimate. Upper limb joint dimensions included in the geometric mean: superoinferior and maximum mediolateral dimensions of the scapular glenoid, articular breadth of the trochlea and capitulum and breadth of the trochlea, and the proximodistal height of the trochlear notch (taken from anterior-most points of the notch), the maximum depth of the trochlea taken perpendicular to the previous measurement, and the anteroposterior length of the coronoid process. For definition of the ulnar metrics, see 14, especially page 303 (see also 15). The radial facet of the ulna of KSD-VP-1/1 is too damaged for accurate measurement and was not included here. For box plot symbol parameters see the legend of Figure S8.

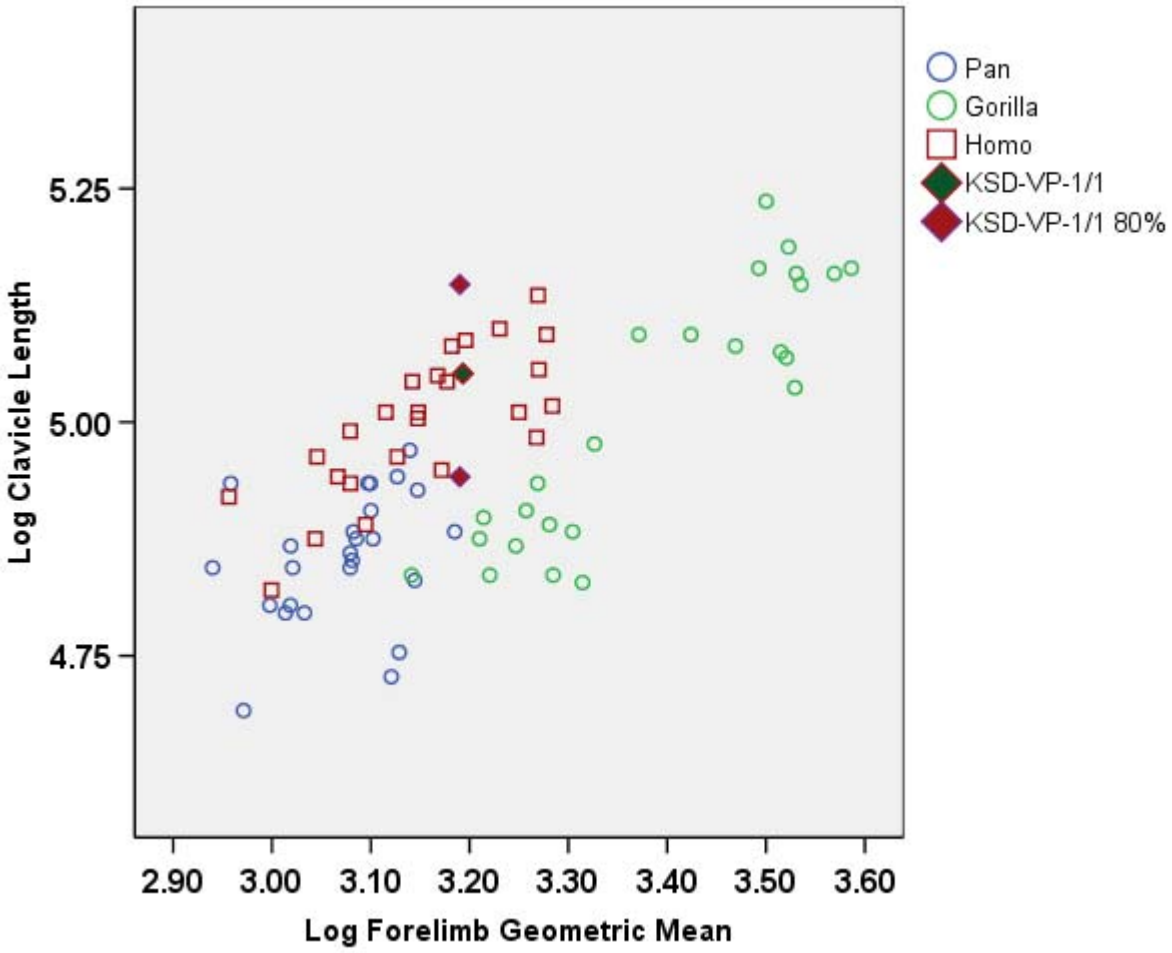

Figure S20. Log-log Scatterplot of Clavicle Length and the Geometric Mean of Eight Joint Dimensions of Scapula, Humerus, and Ulna. KSD-VP-1/1f is most similar to humans, although relative clavicle length does not differ significantly in *Pan* and *Homo*, and the distributions of the two taxa overlap. The 80% confidence limits for the KSD-VP-1/1 regressed length are shown. These suggest more gracile upper limb joints or longer clavicles in early hominids compared to apes, or both, but neither possibility is consistent with a pyramidal cupola. See Figures S28-S30 for variables included in the forelimb geometric mean.

Figure S21. **Scapular Fragments of A.L. 288-1 (left; cast) and an Amerindian of Approximately Equal Size and Preservation.** The specimens are from opposite sides and have been aligned based on the orientations of their glenoid planes. Note the virtual identity of their bar-glenoid angles.

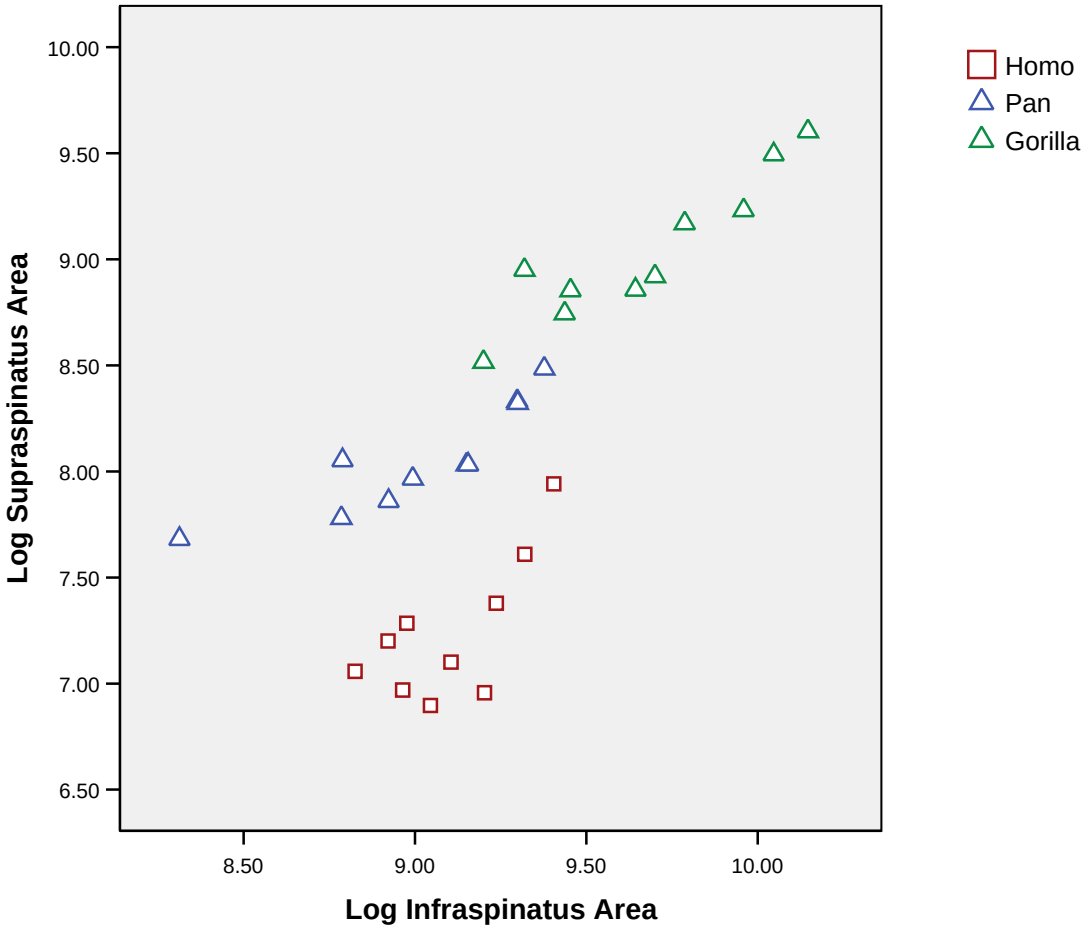

Figure S22. Natural Log-Log Scatterplot of the Areas of the Supraspinous and Infraspinous Fossae from Extant Hominoids. *Homo* exhibits a smaller supraspinous area relative to its infraspinous area than do *Pan* and *Gorilla*. Although insufficient preservation prevents calculation of this ratio in KSD-VP-1/1g, it was likely more similar to those of *Pan* and *Gorilla* based on data from DIK-1-1. However, the dimensions reported for that specimen were simply linear distances. Areas shown here were calculated from X-rays using Image-J. A line was extended from the intersection of the scapular spine and vertebral border of the scapula to the base of the spine near its junction with the glenoid as seen on each X-ray. Each X-ray was made with the scapular blade elevated above the X-ray plate just sufficient to make the glenoid appear as a single broad curved line (cf., Figures 3 and S23). Once the "spine line" was defined and inscribed, the areas of the supraspinous and infraspinous fossae were calculated using the perimeter of the scapular blade as their remaining borders. These same X-rays were also used to calculate the various angles reported in the text and in Table 1.

Figure S23. Definitions of Angles Used to Evaluate Geometry of Hominoid Scapulas. A human scapula is shown here with the five angles used in the PCA described in the text. CD-EF = axillary-vertebral angle; GH-AB = glenoid-spinal angle; AB-IJ = bar-glenoid angle; AB-CD = glenoid-axillary angle; GH-CD = spinal-axillary angle. For discussion see text.

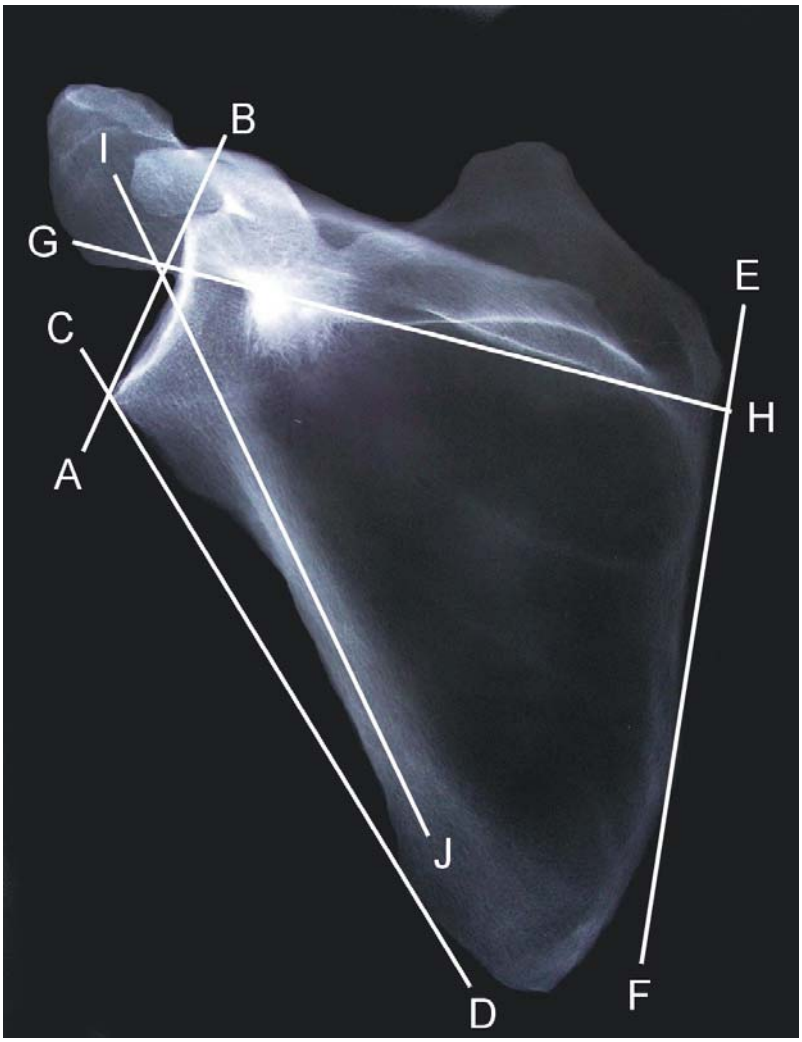

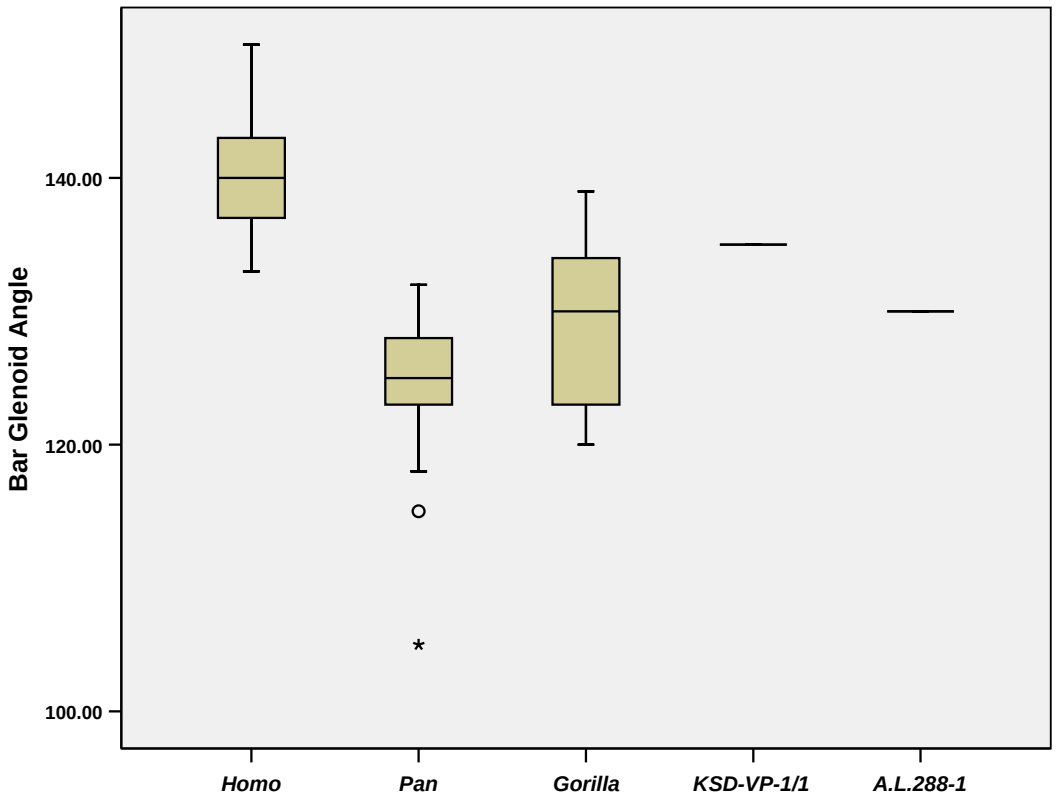

Figure S24. Bar-Glenoid Angle in KSD-VP-1/1g, and in A.L. 288-1, *Pan*, *Gorilla*, and *Homo*. The human sample does not contain the specimen shown in Figure S21. For Box plot parameters see Figure S8. For definitions of angles see Figure S23.

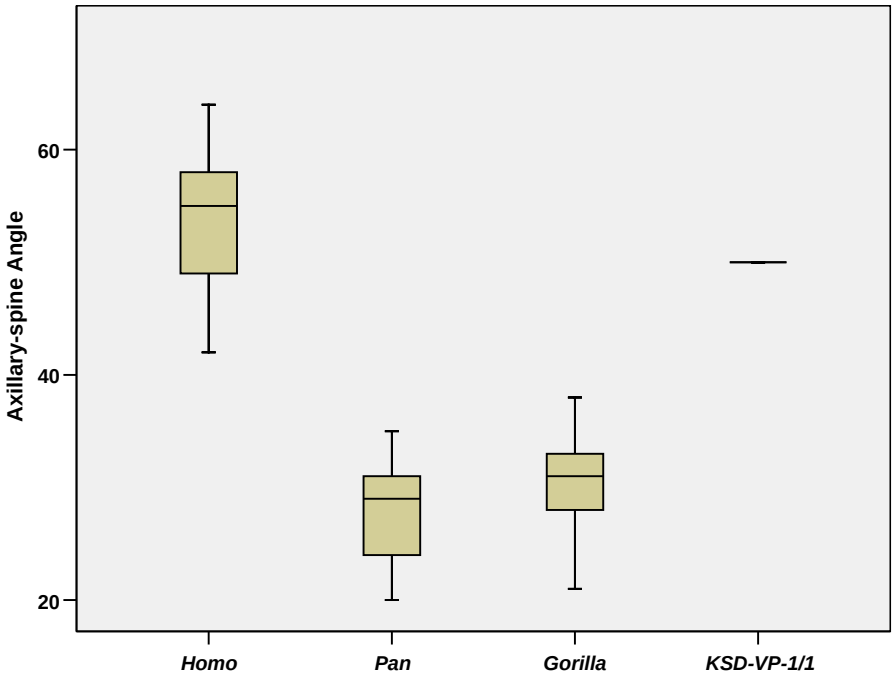

Figure S25. Axillary-Spine Angle in KSD-VP-1/1g, and in *Pan*, *Gorilla*, and *Homo*. For Box plot symbols see Figure S8. For definitions of angles see Figure S23.

Figure S26. Anterior Views of Right Ulna (KSD-VP-1/1a [left]) and Right Humerus (KSD-VP-1/1b [right]). Both specimens have suffered considerable exfoliation of bone from their shaft surfaces. However, the deltopectoral crest of the humerus is clearly rugose. For discussion see text.

Figure S27. Calculation of Trochlear Notch Orientation (TNO) in Incomplete Ulnas (right) and Results for Hominoids and Early Hominids (below). The method used in the present study to measure TNO generally follows that used by Drapeau[14] and Drapeau *et al*.[15] for complete ulnas. Shown here is a measure devised to produce a similar metric from an incomplete ulna[16]. A photograph was taken of the lateral surface of each ulna. The distance from the most proximal point on the olecranon to an anteroposterior tangent applied to the distal edge of the radial facet was measured and doubled. Each photograph was then distally transected at that distance. A best-fit tangent was then applied to the posterior shaft as imaged here (following truncation) and a line connecting the most anterior projections of the coronoid and olecranon portions of the trochlear notch was then inscribed. Angle alpha was calculated and provided in Table S10. The results from this method largely parallel those obtained in 15, although the values listed in Table S10 reported here are higher than those reported in 15 and 16, because shaft curvature tends to reduce the value of the angle. The TNOs of early hominids differ significantly from those of African apes and modern humans, suggesting that an anterior-facing trochlear notch was unique to early hominids. For discussion see text.

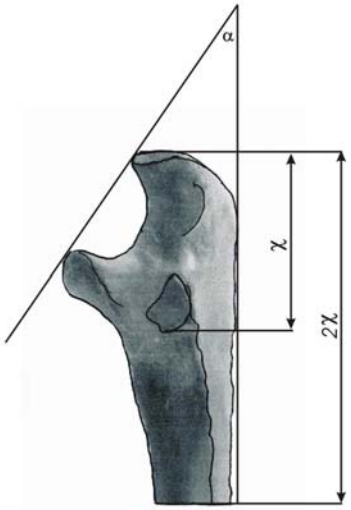

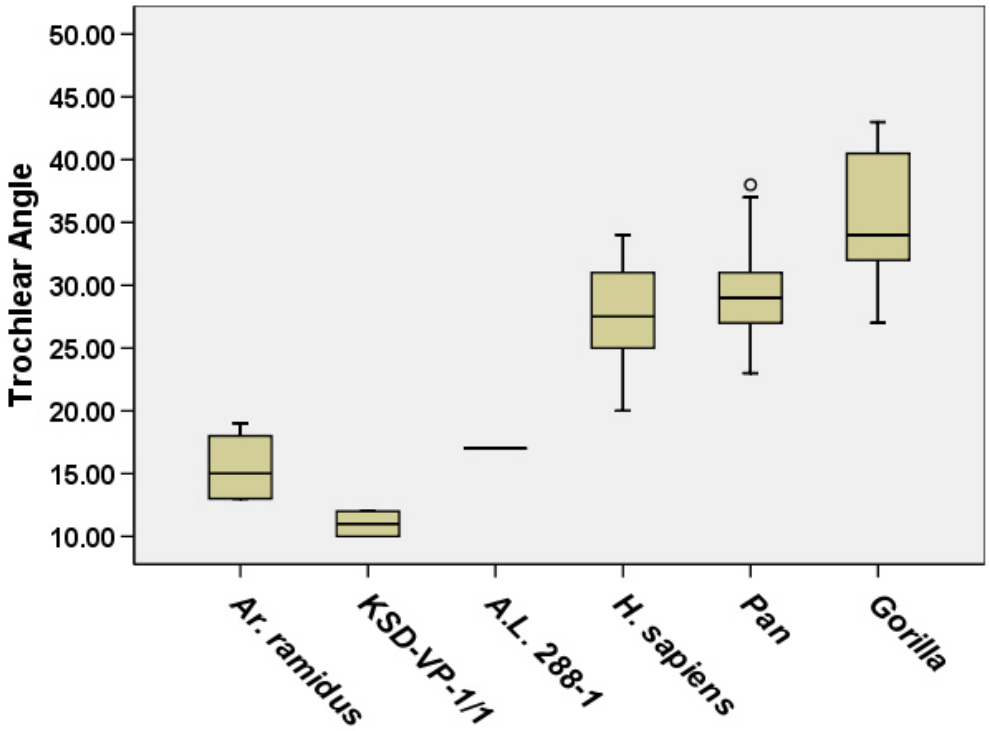

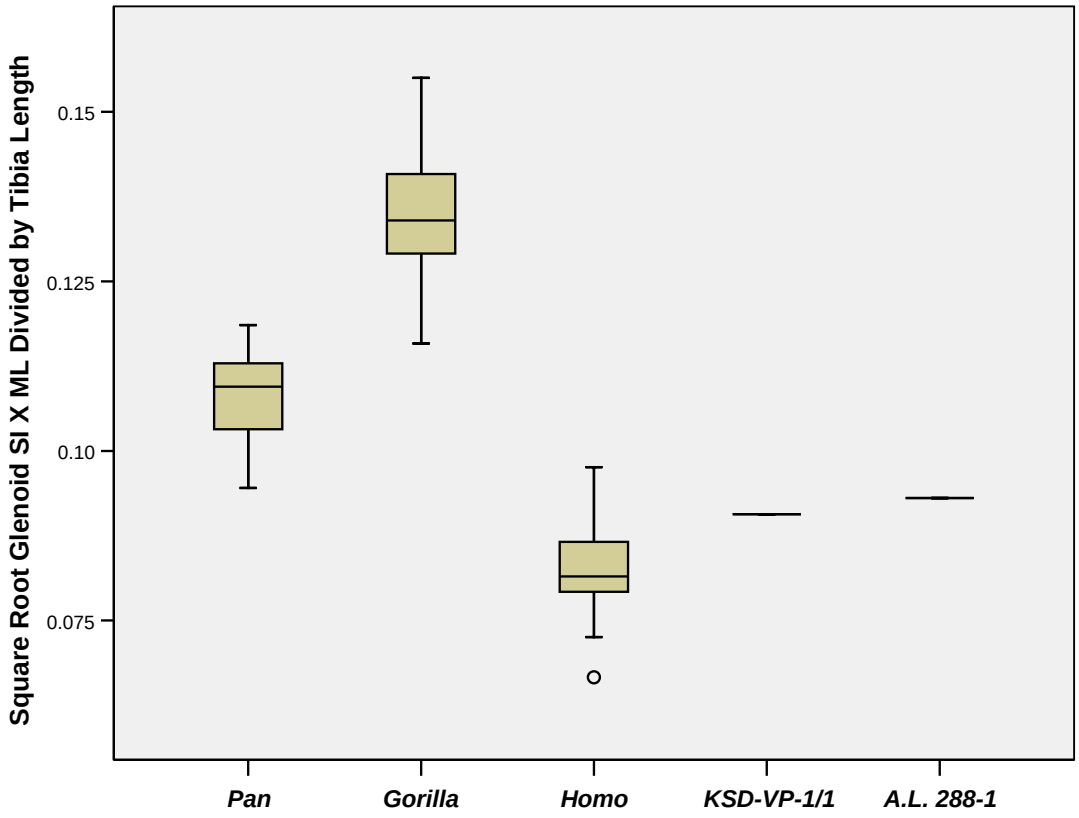

Figure S28. Box plots of Square Root of Superoinferior and Mediolateral Dimensions of the Glenoid Compared to Tibia Length in KSD-VP-1/1 and A.L. 288-1. Tibia length in A.L. 288-1 was calculated using the crural index which varies from 80 to 85 in extant hominoids (cf., Table S12). For box plot parameters see Figure S8. For discussion see text.

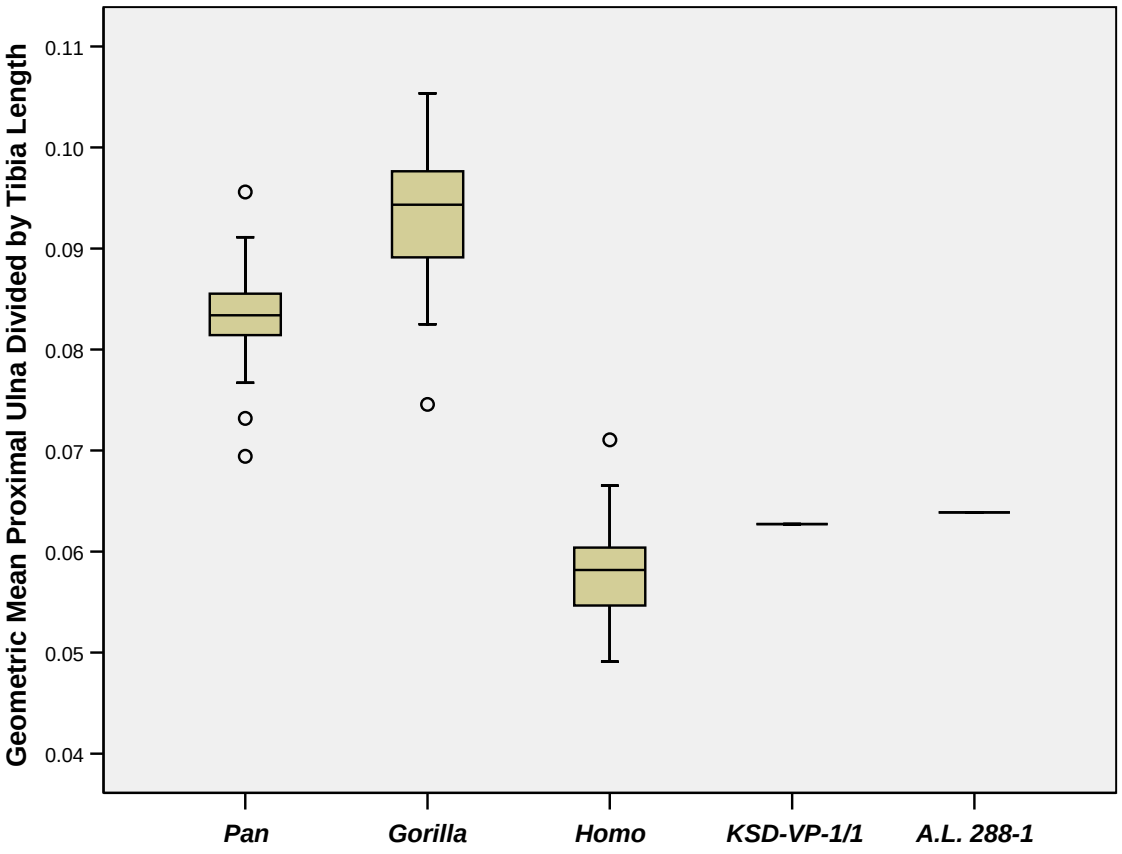

Figure S29. Box plots of Geometric Mean of Proximal Ulnar Metrics Compared to Tibia Length in KSD-VP-1/1 and A.L. 288-1. Tibia length in A.L. 288-1 was calculated using the crural index which varies from 80 to 85 in extant hominoids (cf., Table S12). For box plot parameters see Figure S8. Metrics used for the ulnar geometric mean are the proximodistal height of the trochlear notch, the maximum depth of the trochlea perpendicular to the previous metric, the anteroposterior length of the coronoid process, and the proximodistal height of the olecranon. Each of these is defined in 14 and 15. For discussion see text.

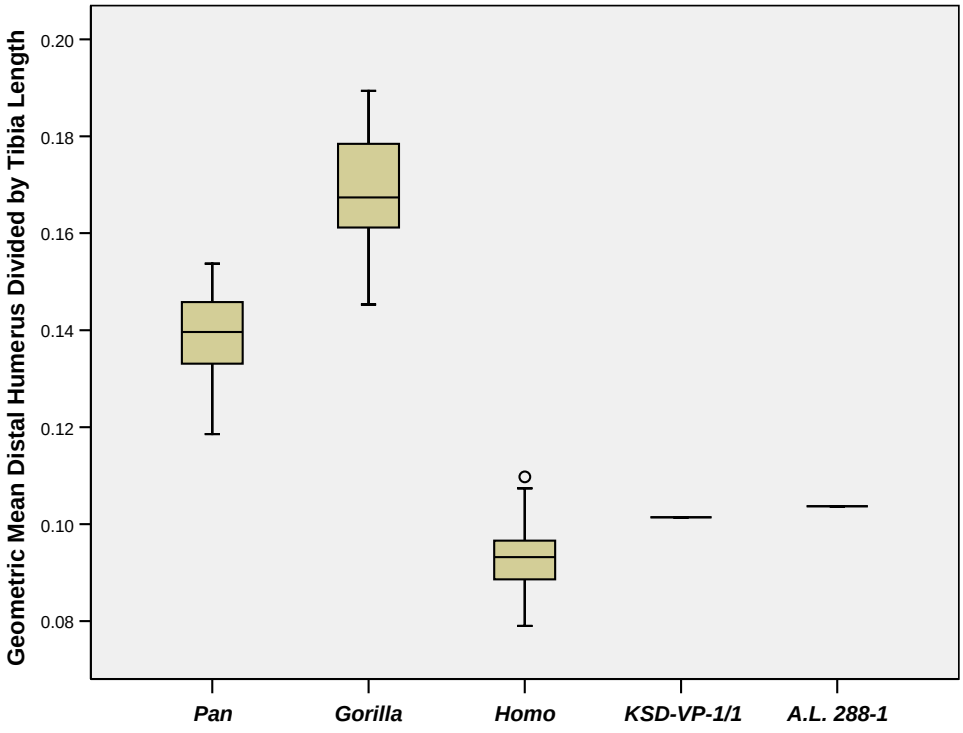

Figure S30. Box plots of Geometric Mean of Distal Humeral Metrics Compared to Tibia Length in KSD-VP-1/1 and A.L. 288-1. Tibia length in A.L. 288-1 was calculated using the crural index which varies from 80 to 85 in extant hominoids (cf., Table S12). For box plot parameters see Figure S8. Metrics used are the maximum transverse breadth of the distal humerus (medial to lateral epicondyles), and mediolateral breadth of the trochlea. For discussion see text.

Table S1
Elements Recovered from the KSD-VP-1/1 Partial Skeleton

Assigned Accession Number	Element
KSD-VP-1/1a	right ulna
KSD-VP-1/1b	right humerus
KSD-VP-1/1c	left distal femur
KSD-VP-1/1d	right innominate
KSD-VP-1/1e	left tibia
KSD-VP-1/1f	left clavicle
KSD-VP-1/1g	right scapula
KSD-VP-1/1h	cervical vertebra
KSD-VP-1/1i	cervical vertebra
KSD-VP-1/1j	cervical vertebra
KSD-VP-1/1k	cervical vertebra
KSD-VP-1/1l	cervical vertebra
KSD-VP-1/1m	vertebral body
KSD-VP-1/1n	left second rib
KSD-VP-1/1o	right lower rib (7th or 8th)
KSD-VP-1/1p	right lower rib (8th or 9th)
KSD-VP-1/1q	right upper rib (5th, 6th or 7th)
KSD-VP-1/1r	left 11^{th} rib
KSD-VP-1/1s	middle rib fragment
KSD-VP-1/1t	superior sacral body and ala
KSD-VP-1/1u	Posterior sacral spine fragment
KSD-VP-1/1v	Sacral spine fragment
KSD-VP-1/1w	coccygeal body?
KSD-VP-1/1x	R. Spinous process with Sup. and Inf. facets
KSD-VP-1/1y	R. Spinous process and Sup. with Inf. facets
KSD-VP-1/1z	R. Spinous process and Sup. with Inf. facets
KSD-VP-1/1aa	L. Spinous process and Sup. with Inf. facets
KSD-VP-1/1ab	L. Spinous process and Sup. with Inf. facets
KSD-VP-1/1ac	L. Spinous process and Sup. with Inf. facets
KSD-VP-1/1ad	vertebral body fragment
KSD-Vp-1/1ae	left superior facet of vertebra
KSD-VP-1/1af	left superior facet of vertebra

Table S2

Lab ID#	J† (X 10^{-3})	± 1σ	^{40}Ar nA‡	±1σ	^{39}Ar nA	±1σ	^{38}Ar nA	±1σ	^{37}Ar nA	±1σ	^{36}Ar nA	±1σ	^{39}Ar Mol × 10^{-14}	Ca/K	±1σ	%^{40}Ar*	Age (Ma)	±1σ§	w/±J ±1σ¶
25333-04	1.841	0.004	88.25983	0.22398	79.82951	0.16031	0.8466	0.04912	0.15829	0.01606	0	0.00174	1.06	0.0038863	0.0003954	100.1	3.671693	0.0261376	0.03
25333-10	1.841	0.004	52.6821	0.16519	46.00955	0.09449	0.40131	0.02127	0	0.0199	0.00827	0.0031	0.61	0	0.0008495	95.3	3.622143	0.0683392	0.07
25333-11	1.841	0.004	43.38917	0.17523	38.06271	0.11044	0.46267	0.02423	0.04544	0.01425	0.00602	0.0017	0.51	0.0023397	0.0007356	95.9	3.627212	0.0488101	0.05
25333-14	1.841	0.004	44.38637	0.14739	38.98933	0.11047	0.36766	0.02523	0.08534	0.01723	0.01028	0.00173	0.52	0.0042902	0.0008683	93.2	3.518709	0.0477044	0.05
25333-20	1.841	0.004	51.84135	0.16427	45.39252	0.13109	0.35921	0.04413	0.14433	0.02133	0.00482	0.00184	0.60	0.006232	0.0009232	97.3	3.685245	0.0442048	0.04
25333-21	1.841	0.004	46.7368	0.17636	40.71901	0.10117	0.34495	0.0282	0.05809	0.01351	0.01	0.00185	0.54	0.0027961	0.0006514	93.7	3.567173	0.0489937	0.05
25333-23	1.841	0.004	46.0717	0.102	42.11056	0.10051	0.50061	0.00996	0	0.11719	0.00452	0.0017	0.43	0	0.0054464	97.1	3.523554	0.0438198	0.04
25334-04	1.842	0.004	34.18083	0.09494	31.16329	0.09017	0.3809	0.00698	0.16356	0.11952	0.00068294	0.00159	0.32	0.0102868	0.0075057	99.4	3.619635	0.0539147	0.05
25334-05	1.842	0.004	25.0029	0.084	23.23503	0.06119	0.29114	0.01025	0	0.12089	0.000486534	0.0015	0.24	0	0.0101826	99.4	3.549278	0.0664784	0.07
25334-06	1.842	0.004	33.30855	0.09168	30.43798	0.08417	0.37038	0.00909	0.04716	0.11839	0.00126	0.0015	0.31	0.0030365	0.007612	98.9	3.591149	0.0520779	0.05
25334-07	1.842	0.004	38.78899	0.11132	35.50694	0.09018	0.40084	0.00967	0	0.11823	0.00307	0.00149	0.37	0	0.0065165	97.6	3.539869	0.0456313	0.05
25334-08	1.842	0.004	30.87228	0.10084	27.95875	0.07721	0.3439	0.01319	0	0.11576	0.00226	0.00156	0.29	0	0.008103	97.8	3.58286	0.0586556	0.06
25334-10	1.842	0.004	39.20211	0.12162	35.96568	0.09123	0.41155	0.00996	0	0.11749	0.00232	0.00156	0.37	0	0.0063928	98.2	3.553133	0.0470806	0.05
25334-11	1.842	0.004	50.40373	0.11182	41.76459	0.12021	0.5033	0.01319	0.05731	0.12185	0.01782	0.00182	0.43	0.0026894	0.0057097	89.6	3.586692	0.0489401	0.05
25334-12	1.842	0.004	30.47951	0.09421	28.03693	0.08324	0.33623	0.01025	0	0.11948	0	0.00157	0.29	0	0.0083397	101.2	3.652188	0.0583552	0.06
25334-14	1.842	0.004	37.31393	0.10006	33.50209	0.08627	0.38516	0.01221	0.02641	0.11882	0.00273	0.00157	0.34	0.0015451	0.0069408	97.8	3.616125	0.0501869	0.05
25334-17	1.842	0.004	45.64501	0.12115	41.70406	0.12018	0.4614	0.01025	0	0.11918	0.00152	0.00142	0.43	0	0.0055927	99.0	3.594302	0.0388046	0.04
25334-18	1.842	0.004	47.8601	0.1111	43.51373	0.08917	0.51045	0.01025	0	0.12182	0.00222	0.00158	0.45	0	0.0054788	98.6	3.598123	0.0398887	0.04
25334-19	1.842	0.004	27.08807	0.08311	24.08838	0.0852	0.30259	0.00726	0.12342	0.11912	0.00292	0.00157	0.25	0.0100426	0.0096773	96.8	3.614063	0.0678606	0.07
25334-20	1.842	0.004	22.25268	0.07838	19.82358	0.04237	0.23722	0.00793	0.12938	0.1188	0.00415	0.00174	0.20	0.0127923	0.0117274	94.5	3.52127	0.08866	0.09
25334-21	1.842	0.004	33.02984	0.08134	25.60127	0.09822	0.28806	0.01123	1.23141	0.12174	0.0154	0.00173	0.26	0.0942749	0.0093142	86.5	3.703922	0.0722012	0.07
25334-22	1.842	0.004	36.08383	0.11163	33.06471	0.11021	0.39273	0.01123	0.23624	0.12382	0.00274	0.00156	0.34	0.0140039	0.0073283	97.8	3.541942	0.0510385	0.05
25334-23	1.842	0.004	48.56331	0.12137	44.53328	0.09723	0.55128	0.01015	0.11138	0.12273	0	0.00172	0.46	0.004902	0.0053929	100.6	3.641466	0.041923	0.04
25334-27	1.842	0.004	31.40278	0.09758	28.7354	0.0982	0.34373	0.0053	0.05373	0.11965	0.000702938	0.00144	0.30	0.0036646	0.0081476	99.3	3.602934	0.0537172	0.05
25334-28	1.842	0.004	41.89841	0.10056	37.91127	0.12017	0.45781	0.01123	0	0.12261	0.00648	0.00161	0.39	0	0.0063289	95.4	3.49902	0.0465836	0.05
														0.0034	**0.0003**		**3.599**	**0.010**	**0.014**※
Omitted, 1.5 nMADs from median age:																			
25333-24	1.841	0.004	39.61836	0.1118	35.39881	0.12048	0.40599	0.0066	0.06426	0.12016	0	0.00162	0.36	0.003558	0.0066432	101.1	3.753589	0.0495933	0.05
25334-02	1.842	0.004	40.44507	0.12143	31.12237	0.11016	0.37847	0.00812	0.18845	0.1185	0.01805	0.00185	0.32	0.0118684	0.0074517	86.8	3.745282	0.0652626	0.07
25334-16	1.842	0.004	42.67736	0.12124	35.97034	0.09722	0.41636	0.01221	0	0.12055	0.00617	0.00175	0.37	0	0.0065589	95.6	3.765722	0.0526052	0.05
Omitted, Age >3.9 Ma:																			
25333-01	1.841	0.004	1259.417	1.10154	142.0966	0.26031	1.5895	0.0561	3.1574	0.03538	0.34324	0.00432	1.89	0.0435514	0.0004987	92.0	26.87475	0.1111502	0.13
25333-03	1.841	0.004	209.5927	0.42252	42.26928	0.12042	0.42172	0.04712	0.10779	0.021	0.47507	0.00491	0.56	0.0049981	0.0009762	33.0	5.430165	0.1735156	0.17
25333-06	1.841	0.004	53.96526	0.1763	38.66976	0.12037	0.40162	0.02028	0.52622	0.01928	0	0.00166	0.51	0.0266718	0.0009835	100.9	4.670833	0.0484956	0.05
25333-07	1.841	0.004	579.3408	0.93112	63.32364	0.13035	0.66155	0.02028	0.98292	0.01901	0.02458	0.00226	0.84	0.0304235	0.0005942	98.8	29.76648	0.1162497	0.13
25333-08	1.841	0.004	781.4986	0.7711	91.05115	0.18028	0.88803	0.04612	0.49532	0.02403	0.00696	0.00235	1.21	0.0106624	0.0005189	99.7	28.21517	0.0985148	0.12
25333-09	1.841	0.004	168.1885	0.29276	23.06899	0.09147	0.24504	0.01537	0.05837	0.01905	0.00933	0.00176	0.31	0.0049589	0.001622	98.4	23.66541	0.1418369	0.15
25333-12	1.841	0.004	337.9193	0.45235	41.77621	0.11045	0.42069	0.02324	0.6256	0.02165	0.00914	0.00195	0.56	0.0293511	0.0010214	99.2	26.46295	0.1138151	0.13
25333-13	1.841	0.004	350.6052	0.61183	38.21838	0.09355	0.34888	0.02919	0.96691	0.02014	0.01115	0.00204	0.51	0.0495872	0.0010439	99.1	29.94338	0.1301264	0.15
25333-15	1.841	0.004	777.7004	0.87137	96.10881	0.18033	1.05141	0.03118	1.92763	0.0247	0.01881	0.00239	1.28	0.0393112	0.0005127	99.3	26.49686	0.0931573	0.11
25333-16	1.841	0.004	432.0739	0.55206	54.02771	0.14049	0.51104	0.03118	0.8048	0.01911	0.00867	0.00223	0.72	0.0291962	0.0006998	99.4	26.21969	0.1093713	0.12
25333-17	1.841	0.004	503.7824	0.68141	62.03749	0.15061	0.74731	0.02324	1.12388	0.02432	0.00131	0.00215	0.82	0.0355078	0.0007761	99.9	26.75937	0.105998	0.12
25333-18	1.841	0.004	663.8292	0.89119	79.88209	0.20065	0.93668	0.02324	1.78245	0.02937	0.03479	0.00224	1.06	0.0437344	0.0007326	98.5	26.97992	0.1091164	0.12
25333-19	1.841	0.004	32.40484	0.16139	1.39	0.02349	0.04493	0.00578	3.29302	0.04739	0.10216	0.0025	0.02	4.643412	0.103697	7.6	5.911413	1.956421	1.96
25333-26	1.841	0.004	6.58308	0.0523	0.88415	0.01864	0.00573	0.00585	2.84786	0.13815	0.01504	0.00286	0.01	6.313226	0.3334766	35.9	8.871007	3.194352	3.19
25334-09	1.842	0.004	124.0601	0.16119	40.02448	0.0942	0.50009	0.00947	0	0.11934	0.12636	0.00312	0.41	0	0.0058351	69.9	7.183602	0.1079205	0.11
25334-13	1.842	0.004	40.91791	0.11182	26.83768	0.08025	0.33821	0.01319	0.45609	0.12736	0.0301	0.00174	0.28	0.0333094	0.0092873	78.3	3.963696	0.073045	0.07
25334-15	1.842	0.004	54.31053	0.10191	44.44169	0.13021	0.52238	0.01015	0.90051	0.12972	0.00489	0.00183	0.46	0.0397148	0.0057136	97.5	3.952427	0.0456884	0.05
25334-24	1.842	0.004	89.94432	0.16099	40.60842	0.11022	0.50895	0.01319	0.31371	0.11952	0.00142	0.00146	0.42	0.0151413	0.0057596	99.6	7.311216	0.0508093	0.05
25334-25	1.842	0.004	346.8136	0.66023	43.13324	0.1502	0.53406	0.01418	0.67918	0.1382	0.00558	0.00311	0.44	0.0308623	0.0062711	99.5	26.39768	0.1602078	0.17
25334-26	1.842	0.004	77.78743	0.16091	34.4729	0.09722	0.40041	0.00996	0.48086	0.1266	0.00806	0.00171	0.35	0.0273399	0.0071868	97.0	7.255971	0.0627336	0.06

NOTES:
†^{40}Ar/^{39}Ar dating neutron fluence parameter.
‡Nanoamps of electron multiplier detector current; all isotopes measured on the same collector.
§Analytical error, not including error in J.
¶Analytical error, including error in J.
※Error expanded by square root of MSWD (Mean Squared Weighted Deviates, = 1.35).
Samples were irradiated for seven hours in the Cd-lined, in-core CLICIT facility of the Oregon State University TRIGA re‡actor. Sanidine from the Fish Canyon Tuff was used as the neutron fluence monitor, with a reference age of 28.201 Ma (Kuiper et al., 2008).

Nucleogenic production ratios:

$(^{36}Ar/^{37}Ar)_{Ca}$	$2.65 \pm 0.022 \times 10^{-4}$
$(^{39}Ar/^{37}Ar)_{Ca}$	$6.95 \pm 0.092 \times 10^{-4}$
$(^{38}Ar/^{37}Ar)_{Ca}$	$0.196 \pm 0.0082 \times 10^{-4}$
$(^{40}Ar/^{39}Ar)_{K}$	$2.5 \pm 0.92 \times 10^{-4}$
$(^{38}Ar/^{39}Ar)_{K}$	$1.22 \pm 0.0027 \times 10^{-2}$
$(^{36}Ar/^{38}Ar)_{Cl}$	3.2×10^{2}
$^{37}Ar/^{39}Ar$ to Ca/K	1.96

Isotopic constants and decay rates:

$\lambda(^{40}K_e)$ /yr	$5.81 \pm 0.17 \times 10^{-11}$
$\lambda(^{40}K_{\beta-})$ /yr	$4.962 \pm 0.086 \times 10^{-10}$
$\lambda(^{37}Ar)$ /d	1.975×10^{-2}
$\lambda(^{39}Ar)$ /d	7.068×10^{-6}
$\lambda(^{36}Cl)$ /d	6.308×10^{-9}
$(^{40}Ar/^{36}Ar)_{Atm}$	295.5 ± 0.5
$(^{40}Ar/^{38}Ar)_{Atm}$	1575 ± 2
$^{40}K/K_{Total}$	0.01167

Table S3
Cardinal Characters of Preserved Portion of the KSD-VP-1/1d Os Coxa Compared to Those of Other Hominoids

Character / Taxon	*Pan*	*Ardipithecus ramidus*	KSD-VP-1/1d	A.L. 288-1	*Homo*
Size and form of Ilium	Narrow superoinferiorly elongated, with narrow g. minimus origin along anterior edge	Substantial anteroposterior expansion including origin of lesser gluteals	Dramatic anteroposterior expansion with extensive origin for lesser gluteals	As in KSD-VP-1/1	As in KSD-VP-1/1 but somewhat anteroposteriorly shorter because of change in birth canal architecture
Size and form of Ischial Tuberosity	Massive, with arc-like undifferentiated hamstring/adductor surface	As in *Pan*	Greatly reduced with marked angulation of hamstring/adductor surface	As in KSD-VP-1/1	As in KSD-VP-1/1 but usually with slightly narrower gap between acetabulum and ischial tuberosity
Lesser sciatic notch	Elongate and only marginally defined	Moderately abbreviated distance between ischial spine and auricular surface with obtuse angulation	Greatly abbreviated distance between ischial spine and auricular surface with narrow acute angulation	As in KSD-VP-1/1 but with less acute angle of notch	Varies with sex. Most Homo males as with KSD-VP-1/1; most females as with A.L. 288-1
Iliac fossa	Narrow, with almost no curvature when viewed from dorsal aspect	Broad but with only minimal sigmoid curvature when viewed from dorsal aspect	Extremely broad with sigmoid curvature when viewed from dorsal aspect	As in KSD-VP-1/1	Less broad than in *Australopithecus* and with more pronounced sigmoid curvature
Sacrum	Very narrow overall and with narrow alae	None preserved	Very broad, with high alae/sacral centrum area ratio	As in KSD-VP-1/1	Broad as in *Australopithecus* but with reduced alae/centrum ratio

Obturator internus groove	None	Locus not preserved but present in likely ancestral forms (*Orriron tugenensis*)	Deep and well defined	As in KSD-VP-1/1	As in KSD-VP-1/1
Iliopsoas groove	None	Moderate in breadth and depth	Deep, well defined, with steep sides	As in KSD-VP-1/1	As in KSD-VP-1/1
AIIS by separate ossification center	No	Adult, but almost certainly	Adult, but almost certainly	Adult, but almost certainly (present in *Au. africanus*)	Yes
Form of Anterior inferior iliac spine (AIIS)	Limited to rugose enthesis with only slight to moderate elevation above iliac surface	Large, sigmoid shaped, projecting	Large, sigmoid shaped, projecting	As in KSD-VP-1/1	As in KSD-VP-1/1
Iliac pillar	None--Expansion only at anterior edge of ilium	Broadly expanded anterior iliac thickness	Anteriorly located and distinct	As in KSD-VP-1/1	Pillar well defined but located more posteriorly
Iliopubic eminence	None	Damaged	Damaged, but highly probable	No	Typical and very frequent
Lunate surface of acetabulum	Covers most of acetabulum except acetabular notch	Damaged	Covers all of acetabulum except acetabular notch	As in KSD-VP-1/1	As in KSD-VP-1/1
Auricular Surface	Highly elongate and very narrow	Damaged	Narrow and moderately elongate	Broader and less elongate; more *Homo*-like	Broad and reniform with distinct superior and inferior demifaces
Acetabulum size	Small to moderate	Small to Moderate	Moderate	As in KSD-VP-1/1	Very large

Retroauricular region	Extremely narrow	Not well preserved but likely narrow	Very broad	Moderate, likely a consequence of body size	Very broad
Superoinferior height of os coxa	Very tall with greatly elongated supra-acetabular terminus	Moderately broad	Short and broad	As in KSD-VP-1/1	As in KSD-VP-1/1
Posterior superior iliac spine	Little or no expansion of iliac crest at posterior terminus	Not preserved	Massive	Much more gracile than KSD-VP-1/1, but likely a consequence of body size	As in KSD-VP-1/1

Table S4
Ratio of Vertical to Horizontal Tangent Lengths of the Lateral Condyle*

Taxon/Specimen	N	Mean Ratio	Range
H. sapiens	15	47.5 (3.9)	41-53
P. troglodytes	15	65.9 (8.2)	55-82
A.L.333-3		46	
A.L. 129-1		48	
KSD-VP-1/1		(52)**	

*Data from 11.
**The lateral condyle has suffered significant damage, though its overall dimensions appear intact. However, the exact location of the meniscal groove must be estimated because of surface damage to the condyle in its most likely location.

TABLE S5
ANALYTICAL TRAIT TYPES

Type 1. A trait that differs in two (or more) taxa because its presence and/or expression are downstream consequences of differences in the positional information of its cells and their resultant effects on local pattern formation. **Type 1** traits are fixed by directional and/or stabilizing selection because their primary functional features have a direct effect on fitness, and result largely from an interaction between genes expressed during morphogenetic field deployment and the functional biology of their adult product. Such traits are particularly subject to modification by changes in the action and or position of enhancers, silencers, and other elements of *cis*, *trans* and mirna regulation.

Example: The superoinferior shortening of the ilium in hominids.

Type 2. A trait that is a collateral byproduct of field changes as in Type 1s, but is *itself* not under direct selection. **Type 2** traits differ in two (or more) taxa because of accumulated differences in positional information (as in Type 1's), but have no functional consequences other than their association with the principally selected character. They may, for example, be the consequence of "hitch-hiking" (selective sweeps). Unlike Types 4 and 5, they do represent true field derived pleiotropy.

Type 2A The antecedent Type 1 is under direct selection which largely determines its frequency;

Type 2B The antecedent Type 1 is not under direct selection (though it may have been so in the past)

Examples: **Type 2A**: Emergence of separate centers of ossification for greater trochanter and femoral head in some mammals--i.e., the principle adaptation being selected is length of the femoral neck[17]. **Type 2B**: Degree of expression of the intertrochanteric line of the human femur. This character varies extensively in human populations and clearly has a genotypic basis, but there is no evidence that it is the result of traction force during ontogeny (i.e., it is not a Type 4), or that it has any impact on the function of the iliofemoral ligament[18].

Type 3. A trait that differs in two taxa because of modification of a systemic growth factor that affects multiple elements, such as an anabolic steroid or systemic expression of cell surface receptors.

Examples: Body size and its allometric effects. Allometric shifts probably reflect differential corporal effects of slight changes of systemic control factors during development. Modulations of Growth Hormone or Insulin-like Growth Factor I (or their receptors)[19]. Specific example: Systemic increase in all elements of the forelimb in *Pongo* and *Hylobates*.

Type 4. A trait that differs between two (or more) taxa because its presence/absence and/or "grade" are attributable exclusively to phenotypic effects of the interaction of "systemic assembly mechanisms"[20] and environmental stimuli. Such traits have no antecedent differences in pattern formation, and therefore have no value in phylogenetic analysis. They are epigenetic and are not pleiotropic. However, they provide significant behavioral information, and are therefore of expository or evidentiary value in interpreting behavior. They often result from habitual behaviors during development.

Examples: The bicondylar angle of the femur; depth of the cotylar fossa of the talus.

Type 5. Traits arising by the same process as Type 4's (phenotypic plasticity) but which have no reliable diagnostic value with respect to behavior. Such traits are not consistently expressed within species and often show marked variation of expression even within individuals of local populations. Example: differential growth of ear size in response to ambient temperature during ontogeny[21]. However, such factors *can* serve as the basis for genetic assimilation.

Table S6
Tibia Length Relative to Acetabular Diameter and Other Metrics in KSD-VP-1/1 and in Other Hominoids (N = 25) Used in This Analysis

Character	KSD-VP-1/1	A.L. 288-1	*H. sapiens*	*P. troglodytes*	*G. gorilla*
Tibia Maximum Length	355	(227-238)¶	376.2 (27.3)	254.3 (12.4)	288.6 (32.1)
Tibia Physiological Length	343		363.1 (27.0)	238.0 (12.0)	271.5 (31.2)
Acetabulum Diameter	(49)*	38***	54.4 (4.4)	40.8 (2.9)	54.3 (6.6)
Femoral Head Diameter	(38)**	28.6	45.7 (4.1)	33.5 (2.3)	45.3 (5.8)
Femoral Length	(418-438)¶	280	460.4 (26.2)	299.0 (14.6)	347.2 (37.1)
Acetabulum/tibia Ratio	.14	(.16 -.17)	.145 (.011)	.161 (.011)	.188 (.012)

*Estimated because of moderate superoinferior crushing
**Average of three estimates; for details see text
***The value listed in 22 is 34.7 but represents the inside diameter; the method used here is that described by C.V. Ward[23]
¶Estimated by crural indexes of 81 and 85

Table S7

Metric Parameters of Distal Tibia in Hominoids from DeSilva (5,6, Personal Communication) and this study for KSD-VP-1/1

Taxon		Malleolar Shape Index (AP ÷ ML)/100		Plafond Declination Angle (PDA)		Relative Articular Surface Depth		Metaphyseal Shape Index (AP ÷ ML)/100	
	N	Mean (SD)	Range	Mean (SD)	Range	Mean (SD)	Range	Mean (SD)	Range
Gorilla	44	68.3 (5.2)	56.7-84.5	105.6 (2.5)	99.3-110.0	12.0 (2.6)	7.9-17.7	63.7 (4.7)	52.7-72.5
Pan	53	72.2 (6.5)	55.7-90.2	102.7 (4.2)	94.5-112.7	12.3 (2.3)	7.6-17.2	69.5 (4.9)	58.6-83.8
H. sapiens	69	54.5 (5.2)	39.0-64.4	91.1 (2.4)	86.1-96.5	16.1 (1.7)	11.5-19.4	82.2 (4.8)	74.6-94.2
A. afarensis	3	59.1 (2.6)	56.1-60.6	90.8 (0.69)	90.0-91.2	16.6 (0.8)	16.0-17.5	85.8 (6.9)	81.0-93.8
A. anamensis	1	52.1		93.1		17.9		84.5	
Other early hominids	7-9¶	56.2 (5.6)	49.6-65.6	91.0 (2.5)*	87.4-94.7*	14.8 (1.6)	10.4-17.8	89.1 (7.6)	80.7-100.3
KSD-VP-1/1		47		100**		(20)**		100	

¶Varies: for details see 5,6.
*Excludes pathological specimen (probable fibular fracture) KNM-ER-2596.
**Impacted by probable sequelae to remote fibular fracture (see text).

Table S8
Absolute and Relative Clavicular Length and Circumference in Hominoids

Taxon*	Clavicle Length	Mid-Clavicle Circum.	Length/Geometric Mean Upper Limb	Circum./ Geometric Mean Upper Limb
Pan	128.7 (8.8)	35.8 (2.1)	4.7 (0.34)	1.3 (0.07)
Gorilla	151.2 (20.6)	43.2 (7.9)	4.1 (0.24)	1.2 (0.12)
Homo	148.7 (11.3)	39.2 (4.6)	5.2 (0.32)	1.4 (0.12)
KSD-VP-1/1f	156.4**	46	5.3	1.6

*N for each taxon = 25
**Estimated by regression; likely a minimum value

Table S9
Humerus Metrics for Extant Hominoids, KSD-VP-1/1 and A.L. 288-1

Taxon*	Distal Articular Breadth	Trochlea Breadth	Humerus Max. Length
P. troglodytes	45.7 (13.0)	27.2 (2.3)	306.9 (14.9)
G. gorilla	61.0 (8.8)	39.2 (6.4)	411.9 (40.1)
H. sapiens	44.9 (4.6)	27.3 (2.9)	324.8 (20.8)
KSD-VP-1/1b	46-48	27	
A.L. 288-1	30.1	19.3	235

*N for each taxon = 25

Table S10
Ulnar Metrics in Anthropoids*

Taxon	Olecranon Orientation (OO) Mean (S.D.)*	Proximodistal height of olecranon (OH) Mean (S.D.)*	Keeling Angle (UKN) Mean (S.D.)*	Trochlear Notch Orientation (UNO) Mean (.S.D.)*	Trochlear Notch Orientation: Proximal Ulna (this study) N = 15 each taxon**
H. sapiens	110.0 (7.3)	4.2 (1.5)	123 (8)	21.4 (5.5)	27.3 (3.8)
P. troglodytes	102.0 (7.2)	3.5 (2.3)	105 (8)	20.5 (7.7)	29.8 (4.9)
P. paniscus	105.4 (5.7)	2.0 (2.5)	109 (10)	19.9 (3.8)	
Gorilla	97.4 (7.0)	1.9 (2.3)	116 (7)	27.3 (5.2)	35.3 (5.6)
A.L. 288-1	118	5.1	131	9/10[¶]	17
OH-36	122/125[***]	12	102	7/10	
L40-19 (Omo)	111	5.1	121	2/9.5	
A.L. 438-1	125	7.7	131	10.5/13.3	
KSD-VP-1/1		7.5	126		10-12
BOU-VP-12/1	127-132	5.5	120	5/8	16
ARA-VP-7/2-C					19[#]
ARA-VP-6/500-051					14[#]

*Data from 14,15, except where noted. OO: "olecranon orientation measured as the angle between the axis of olecranon length and the long axis of the bone"; OH: "proximodistal olecranon height measured from the anterior tip of the anconeal process" UKN: Keeling of trochlear notch measured as the angle between the articular processes of the trochlear notch on each side of the keel on the proximal part of the trochlear notch; UNO: Trochlear notch orientation measured as the angle between two lines; one drawn between the two anterior-most points of the anconeal and coronoid processes, and the other between the deepest point on the trochlear articular surface and the center of the ulnar head (15: p. 609).

**UNO values are lower in complete ulnas as a consequence of diaphyseal curvature--compare method described in Figure S27 to Fig 14 in 15.

***Paired values for single individuals are minima and maxima.

[#]Values are estimates (for details see Figure S32 in 16)

[¶]Values from 14 (i.e., 9) and this study (i.e., 10) were obtained by using methods described in 14, and were reported in Table S5 of 16. The values plotted in Figure S27 of this study (and in Figure S32 of 16) are by methods described here (and in 16) for evaluation of *incomplete* ulnas. See also note **.

Table S11
Humerus/Femur Ratio in Hominoids

Taxon	**N**	**Mean**
H. sapiens	29	71.2 (2.20)
P. troglodytes	30	101.7 (3.01)
G. gorilla	29	116.4 (3.96)
P. pygmaeus	19	130.1 (3.13)
H. lar	14	116 (2.06)
A.L. 288-1		84

Table S12
Crural Index* in Hominoids (N =50 each taxon)

Taxon	Mean
H. sapiens	.816 (.038)
P. troglodytes	.847 (.019)
G. gorilla	.829 (.023)
Mean: all three taxa	.831

*Tibia maximum length divided by femur maximum length.

References

1. Deino A, *et al.* (2010) $^{40}Ar/^{39}Ar$ dating, paleomagnetism, and tephrochemistry of Pliocene strata of the hominid-bearing Woranso-Mille area, west-central Afar Rift, Ethiopia. *J Hum Evol* 58: 111-126.

2. Haile-Selassie Y, *et al.* (2007) Preliminary geology and paleontology of the Woranso-Mille, Central Afar, Ethiopia. *Anthro Sci* 115: 215-222.

3. Gradstein FM, Ogg JG, Smith AG (2004) *A Geologic Time Scale* (Cambridge University Press, Cambridge) pp. 1-589.

4. Lovejoy CO (2005) The natural history of human gait and posture 1: spine and pelvis. *Gait and Posture* 21: 95-112.

5. DeSilva JM (2008) Ph.D. University of Michigan.

6. DeSilva JM (2009) Functional morphology of the ankle and the likelihood of climbing in early hominins. *Proc Natl. Acad. Sci. U. S. A.* 106: 6567-6572.

7. Wiltse LL (1972) Valgus Deformity of the Ankle: A sequel to the acquired or congenital abnormalities of the fibula. *J. Bone Joint Surg Am* 54A: 595-606.

8. Simpson SW, *et al.*, (2008) A female *Homo erectus* pelvis from Gona, Ethiopia. *Science* 322: 1089-1092.

9. Tague RG, Lovejoy CO (1998) AL 288-1--Lucy or Lucifer: gender confusion in the Pliocene. *J Hum Evol* 35: 75-94.

10. Robinson JT (1972) *Early Hominid Posture and Locomotion* (University of Chicago Press, Chicago).

11. Lovejoy CO (2007) The natural history of human gait and posture 3: Knee. *Gait and Posture* 25: 325-341

12. Jellima LM, Latimer B, Walker A (1993) The rib cage. in: *The Nariokotome Homo erectus skeleton* (WalkerA, Leakey REF, Eds). (Harvard Univ. Press, Cambridge, Ma.) pp. 294-325.

13. Asfaw B, *et al*., (1999) *Australopithecus garhi*: A new species of early hominid from Ethiopia. *Science* 284: 629-634.

14. Drapeau MS (2004) Functional anatomy of the olecranon process in hominoids and plio-pleistocene hominins. *Am J Phys Anthropol* 124: 297-314.

15. Drapeau MS, *et al.* (2005) Associated cranial and forelimb remains attributed to Australopithecus afarensis from Hadar, Ethiopia. *J Hum Evol* 48: 593-642.

16. Lovejoy CO, *et al.* (2009) Careful climbing in the Miocene: the forelimbs of Ardipithecus ramidus and humans are primitive. *Science* 326, 70: 70e1.

17. Serrat MA *et al.* (2007) Variation in mammalian proximal femoral development: comparative analysis of two distinct ossification patterns. *J Anat* 210: 249-258.

18. Lovejoy CO, Heiple, KG (1971) The proximal femoral anatomy of *Australopithecus*. *Nature* 235:175-176,

19. Serrat MA, Lovejoy CO, King D (2007) Age- and site-specific decline in insulin-like growth factor-I receptor expression is correlated with differential growth plate activity in the mouse hindlimb. *Anat. Rec. (Hoboken.)* 290: 375-381.

20. Lovejoy CO, Cohn MJ, White TD (1999) Morphological analysis of the mammalian postcranium: A developmental perspective. *Proc. Nat. Acad. Sci.* 96: 13247-13252.

21. Serrat MA, King D, Lovejoy CO (2008) Temperature regulates limb length in homeotherms by directly modulating cartilage growth. *Proc Nat Acad Sci* 105: 19348-19353.

22. Johanson DC, *et al.* (1982) Morphology of the Pliocene partial hominid skeleton (A.L. 288-1) from the Hadar Formation, Ethiopia. *Am J Phys Anthro* 57: 403-451.

23. Ward CV (1991) Ph.D. Johns Hopkins.